JEM Journal of Experimental Medicine

ARTICLE

Human *STAT3* variants underlie autosomal dominant hyper-IgE syndrome by negative dominance

Takaki Asano[1], Joëlle Khourieh[2,3*], Peng Zhang[1*], Franck Rapaport[1*], András N. Spaan[1], Juan Li[1], Wei-Te Lei[1], Simon J. Pelham[1], David Hum[1], Maya Chrabieh[2,3], Ji Eun Han[1], Antoine Guérin[4,5], Joseph Mackie[4,5], Sudhir Gupta[6], Biman Saikia[7], Jamila E.I. Baghdadi[8], Ilham Fadil[9,10], Aziz Bousfiha[9,10], Tanwir Habib[11], Nico Marr[11,12], Luckshman Ganeshanandan[13], Jane Peake[14], Luke Droney[15], Andrew Williams[16], Fatih Celmeli[17], Nevin Hatipoglu[18], Tayfun Ozcelik[19], Capucine Picard[20,21,22,23], Laurent Abel[1,2,3], Stuart G. Tangye[4,5], Stéphanie Boisson-Dupuis[1,2,3], Qian Zhang[1,2,3**], Anne Puel[1,2,3**], Vivien Béziat[1,2,3**], Jean-Laurent Casanova[1,2,3,24***], and Bertrand Boisson[1,2,3***]

Most patients with autosomal dominant hyper-IgE syndrome (AD-HIES) carry rare heterozygous *STAT3* variants. Only six of the 135 in-frame variants reported have been experimentally shown to be dominant negative (DN), and it has been recently suggested that eight out-of-frame variants operate by haploinsufficiency. We experimentally tested these 143 variants, 7 novel out-of-frame variants found in HIES patients, and other *STAT3* variants from the general population. Strikingly, all 15 out-of-frame variants were DN via their encoded (1) truncated proteins, (2) neoproteins generated from a translation reinitiation codon, and (3) isoforms from alternative transcripts or a combination thereof. Moreover, 128 of the 135 in-frame variants (95%) were also DN. The patients carrying the seven non-DN *STAT3* in-frame variants have not been studied for other genetic etiologies. Finally, none of the variants from the general population tested, including an out-of-frame variant, were DN. Overall, our findings show that heterozygous *STAT3* variants, whether in or out of frame, underlie AD-HIES through negative dominance rather than haploinsufficiency.

Introduction

Hyper-IgE syndrome (HIES) is an inborn error of immunity (IEI), initially described as Job's syndrome by Davis et al. in 1966 for patients with recurrent "cold" staphylococcal abscesses, eczema, and respiratory infections beginning at birth (Davis et al., 1966). In 1972, Buckley et al. reported high serum IgE levels in patients with this condition, which was renamed HIES (Buckley et al., 1972). These patients also have other clinical manifestations, including eosinophilia, low levels of inflammatory markers during infection, chronic mucocutaneous candidiasis (CMC), systemic allergic manifestations, and extra-hematopoietic features, including facial dysmorphism, deciduous tooth retention, osteopenia, hyperextensibility, scoliosis, and vascular abnormalities (Chandesris et al., 2012; Grimbacher et al., 1999; Tsilifis et al., 2021; Zhang et al., 2018b) The manifestations of HIES display variable expressivity. The estimated frequency of HIES is between 1 per 100,000 to 1,000,000 at

[1]St. Giles Laboratory of Human Genetics of Infectious Diseases, Rockefeller Branch, The Rockefeller University, New York, NY; [2]Paris University, Imagine Institute, Paris, France; [3]Laboratory of Human Genetics of Infectious Disease, Necker Branch, Institut National de la Santé et de la Recherche Médicale U1163, Paris, France; [4]Garvan Institute of Medical Research, Darlinghurst, Australia; [5]St. Vincent's Clinical School, Faculty of Medicine and Health, University of New South Wales, Sydney, Australia; [6]Division of Basic and Clinical Immunology, Department of Medicine, School of Medicine, University of California, Irvine, Irvine, CA; [7]Department of Immunopathology, Post Graduate Institute of Medical Education and Research, Chandigarh, India; [8]Genetics Unit, Military Hospital Mohamed V, Rabat, Morocco; [9]Laboratory of Clinical Immunology, Inflammation and Allergy, Faculty of Medicine and Pharmacy of Casablanca, King Hassan II University, Casablanca, Morocco; [10]Clinical Immunology Unit, Department of Pediatric Infectious Diseases, Children's Hospital, Averroes University Hospital Center, Casablanca, Morocco; [11]Research Branch, Sidra Medicine, Qatar Foundation, Doha, Qatar; [12]College of Health & Life Sciences, Hamad Bin Khalifa University, Qatar Foundation, Doha, Qatar; [13]Department of Clinical Immunology, PathWest Laboratory Medicine Western Australia, Fiona Stanley Hospital, Perth, Australia; [14]Queensland Children's Hospital, South Brisbane, Australia; [15]Department of Clinical Immunology, Princess Alexandra Hospital, Brisbane, Australia; [16]Immunology Laboratory, Children's Hospital Westmead, Westmead, Australia; [17]Department of Allergy and Immunology, University of Medical Science Antalya Education and Research Hospital, Antalya, Turkey; [18]Bakirkoy Dr Sadi Konuk Education and Training Hospital, Istanbul, Turkey; [19]Department of Molecular Biology and Genetics, Bilkent University, Ankara, Turkey; [20]Université de Paris, Paris, France; [21]Study Center for Primary Immunodeficiencies, Hôpital Necker-Enfants Malades, Assistance Publique-Hôpitaux de Paris, Paris, France; [22]Laboratory of Lymphocyte Activation and Susceptibility to EBV Infection, Institut National de la Santé et de la Recherche Médicale UMR 1163, Imagine Institute, Paris, France; [23]Pediatric Immunology-Hematology Unit, Assistance Publique-Hôpitaux de Paris, Necker Hospital for Sick Children, Paris, France; [24]Howard Hughes Medical Institute, New York, NY.

*J. Khourieh, P. Zhang, and F. Rapaport contributed equally to this paper; **Q. Zhang, A. Puel, and V. Béziat contributed equally to this paper; ***J.-L. Casanova and B. Boisson contributed equally to this paper; Correspondence to Jean-Laurent Casanova: jean-laurent.casanova@rockefeller.edu; Bertrand Boisson: bebo283@rockefeller.edu.

birth (Ghaffari, 2018; Mogensen, 2013). However, its actual prevalence may be higher due to the incomplete penetrance of most of its clinical manifestations. HIES is typically inherited as an autosomal dominant (AD) trait (Grimbacher et al., 1999). The first genetic etiology to be identified, monoallelic dominant-negative (DN) missense variants of signal transducer and activator of transcription 3 (*STAT3*), was reported in 2007 and accounts for >90% of sporadic and familial cases (Minegishi et al., 2007). Three other genetic etiologies have since been reported; all three are almost undistinguishable phenocopies of AD STAT3 deficiency: (1) autosomal recessive (AR) ZNF341 deficiency (ZNF341 being a transcription factor required for the expression and activity of STAT3; Béziat et al., 2018; Frey-Jakobs et al., 2018), (2) AR partial deficiency of the common receptor chain gp130 (encoded by *IL6ST*; Schwerd et al., 2017), and (3) DN *IL6ST* variants in other kindreds with a typical form of AD-HIES (Béziat et al., 2020). The unifying mechanism underlying most clinical features is the disruption of IL-6– and IL-11–dependent STAT3 activation. Patients with AR complete IL-6R deficiency (Spencer et al., 2019) have a closely related phenotype, without extrahematopoietic manifestations, whereas patients with AR IL-11R deficiency (Keupp et al., 2013) lack the hematological manifestations.

By July 2020, 143 heterozygous variants of *STAT3* had been reported to underlie HIES (Abolhassani et al., 2018; Al Khatib et al., 2009; Alcántara-Montiel et al., 2016; Anolik et al., 2009; Avery et al., 2010; Chandesris et al., 2012; Egawa et al., 2019; Eken et al., 2020; Felgentreff et al., 2014; Freeman et al., 2013; Giacomelli et al., 2011; Hagl et al., 2016; He et al., 2012; Heimall et al., 2011; Holland et al., 2007; Jiao et al., 2008; Khourieh et al., 2019; Kim et al., 2009; Kumánovics et al., 2010; Larsen et al., 2019; Ma et al., 2012; Ma et al., 2008; Merli et al., 2014; Minegishi et al., 2009; Minegishi et al., 2007; Miyazaki et al., 2011; Moens et al., 2017; Moens et al., 2014; Mogensen, 2013; Natarajan et al., 2018; Papanastasiou et al., 2010; Pelham et al., 2016; Powers et al., 2009; Renner et al., 2008; Renner et al., 2007; Robinson et al., 2011b; Schimke et al., 2010; Sundin et al., 2014; van de Veerdonk et al., 2010; Vinh et al., 2010; Woellner et al., 2010; Wolach et al., 2014; Wu et al., 2017; Zhang et al., 2013). These 143 variants include 114 (79%) missense mutations, 21 (15%) in-frame indels, and 8 (6%) nonsense or frameshift indels. Only 6 variants, all in-frame, were experimentally shown to be both loss of function (LOF) and DN (Khourieh et al., 2019; Minegishi et al., 2007). In the remaining 137 variants, 129 of which were in-frame variants (the remaining 8 being out-of-frame variants), the mechanism of autosomal dominance was not experimentally tested. Only 20 of these variants have actually been shown to be LOF. The 129 in-frame variants are thus assumed, but not proven, to be DN. The recent reports of eight nonsense and frameshift variants predicted to be LOF in HIES patients were surprising (Anolik et al., 2009; Natarajan et al., 2018; Renner et al., 2008; Tavassoli et al., 2019; Woellner et al., 2010). It was suggested that one of these variants (c.1140-3C>G; p.S381*) caused atypical AD-HIES by haploinsufficiency (HI) rather than DN, because it led to a premature stop codon and the amount of STAT3 protein in the patient's T cells was half that in healthy donors (Natarajan et al., 2018). This report challenged the long-standing paradigm that heterozygous *STAT3* variants cause HIES by negative dominance. However, negative dominance was not experimentally excluded (Natarajan et al., 2018). Overall, there is suggestive but inconclusive evidence to suggest that (1) heterozygous loss-of-expression variants of *STAT3* can cause HIES and (2) the autosomal dominance underlying HIES can operate both by negative dominance and by HI mechanisms. We addressed both these issues by experimentally testing all known *STAT3* variants found in HIES patients, including known and novel variants predicted to be loss of expression (pLOF), and selected variants found in the general population.

Results

Seven families with AD-HIES and *STAT3* nonsense or frameshift variants pLOF

In our in-house cohort of patients with HIES, we identified seven new individuals from five families with previously unknown nonsense or frameshift variants of *STAT3* (P1–P7; Fig. 1 A). These seven patients (P1, P2, P3, P4, P5, P6, and P7) were diagnosed with classical HIES on the basis of signs such as high serum IgE levels, recurrent skin abscesses, and recurrent pneumonia (Table S1; see case reports in Materials and methods). All of these patients carried private heterozygous nonsense or frameshift variants of *STAT3* [P1: c.373C>T (p.Q125*), P2: c.1111_1112del (p.D371Lfs*14), P3: c.1552C>T (p.R518*), P4 and P5: c.1685G>A (p.W562*), P6 and P7: c.1897C>T (p.Q633*)]. They had no biallelic rare variants of *DOCK8*, *PGM3*, *IL6ST*, *IL6R*, and *ZNF341* or monoallelic rare variants of *CARD11*, *ERBBIP2*, *IL6ST*, or *TGFBR1/2*, which underlie HIES, as broadly defined in the 2019 classification of the International Union of Immunological Societies Expert Committee (August, 2018; Béziat et al., 2018; Béziat et al., 2020; Bousfiha et al., 2020; Engelhardt et al., 2009; Felgentreff et al., 2014; Fleisher, 2014; Frey-Jakobs et al., 2018; Lyons et al., 2017; Ma et al., 2017; Sassi et al., 2014; Schwerd et al., 2017; Spencer et al., 2019; Su, 2010; Tangye et al., 2020; Zhang et al., 2010b; Zhang et al., 2009; Zhang et al., 2014). These five new nonsense and frameshift *STAT3* variants (Fig. 1 A) were not found in the Human Gene Mutation Database of pathological variants, the 1,000 Genomes Project, or Genome Aggregation Database (gnomAD). The screening of our whole cohort (>8,000 individuals with severe or recurrent infections) led to the identification of another three individuals (P8, P9, and P10) from two kindreds with two previously unknown frameshift variants [P8 and P9: c.2091delT (p.D698Tfs*9), P10: c.2090ins22 (p.D698Efs*6); Fig. 1 A]. P8, P9, and P10 were diagnosed with nonclassical HIES due to their atypical clinical manifestations, with only slightly high serum IgE levels and without CMC or connective tissue disorders, resulting in lower National Institutes of Health (NIH) scores than for P1–P7 (Table S1). They also suffered from tuberculosis (TB), which has rarely been reported in patients with HIES (Ashtekar and Shah, 2016; Grimbacher et al., 2005; Metin et al., 2004). We analyzed the predicted deleteriousness of all variants (P1–P10). All their combined annotation-dependent depletion (CADD) scores were above the 99% confidence threshold for the mutation significance cutoff (MSC) for *STAT3* (16.4; Fig. 1 B; Itan et al., 2016; Rentzsch et al., 2019; Zhang et al., 2018a). These results also suggest that the nonsense or

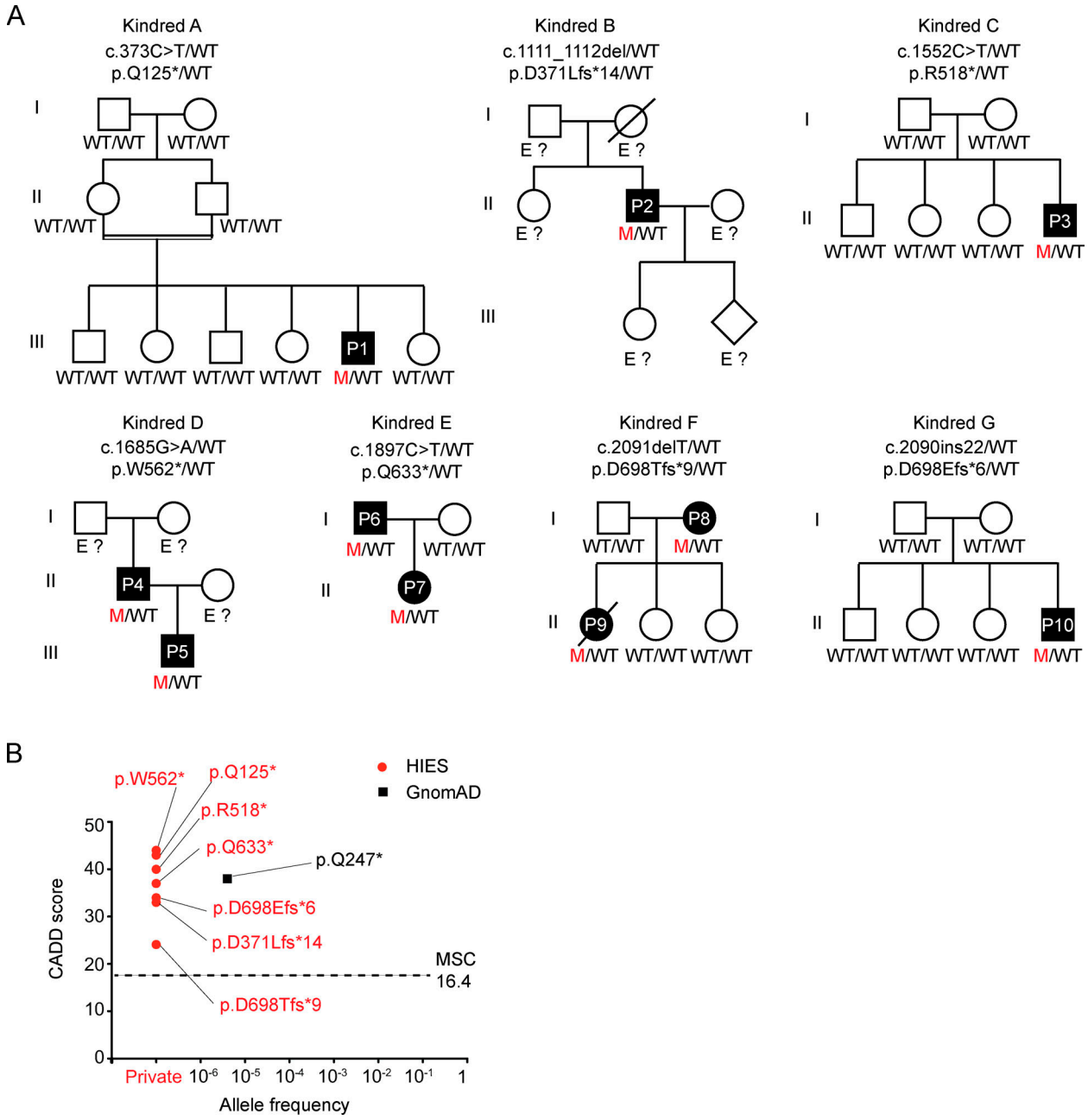

Figure 1. ***STAT3* nonsense or frameshift variants in HIES. (A)** Pedigree of the seven unrelated families showing familial segregation of *STAT3* nonsense or frameshift variants in our cohort. M, mutant. Individuals of unknown genotype are labeled "E?". **(B)** Graph showing the predicted CADD scores (v1.6; Kircher et al., 2014; Rentzsch et al., 2019) and global allele frequency of the nonsense or frameshift variants found in the patients with HIES (red circles) and nonsense variants of *STAT3* (black squares) found in the heterozygous state in the gnomAD database. The CADD-MSC score (99% confidence interval) for *STAT3* is indicated by a black dashed line.

frameshift variants of *STAT3* predicted to be LOF may be responsible for AD-HIES.

13 out-of-frame *STAT3* variants are DN because they encode truncated proteins

We assessed the potential impact of nonsense or frameshift variants in terms of the molecular mechanism of dominance. We studied the mechanism of dominance not only for the seven nonsense or frameshift variants in our cohort but also for the eight reported variants (Fig. 2 A). Three of the eight reported variants (c.1140-2A>C, c.1140-2A>G, and c.1140-3C>G), all affecting the same splice site, were predicted to create an identical transcript (S381*). We thus assessed the STAT3 activity of the 13 cDNAs corresponding to these 15 variants in a luciferase assay. We used an empty plasmid (empty vector [EV]), WT STAT3, or each variant cDNA to transfect a *STAT3*-deficient epithelial DLD1 colon carcinoma cell line (*STAT3*$^{-/-}$ A4), together with a *STAT3*-specific luciferase reporter, and we measured luciferase activity.

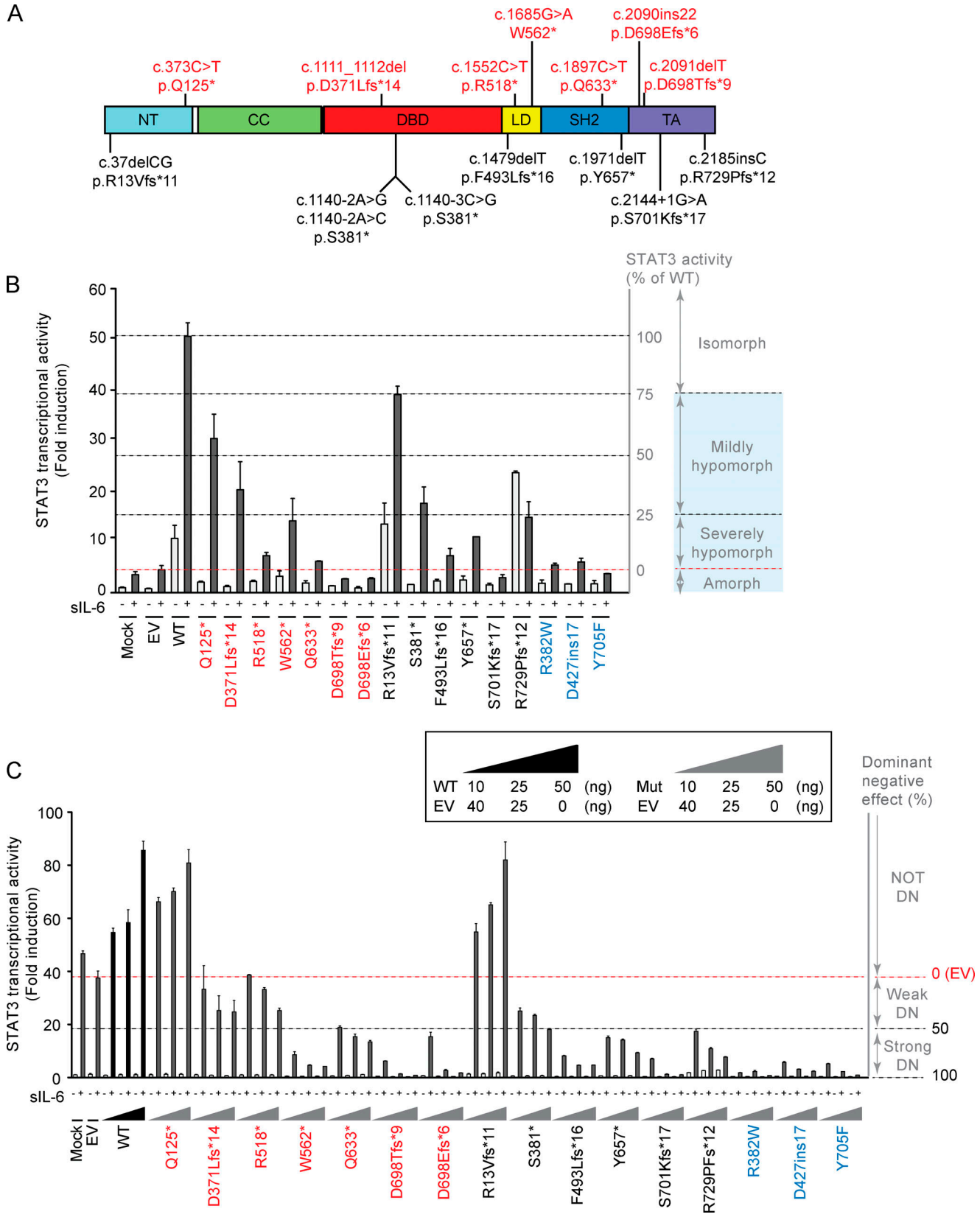

Figure 2. **Allele activity and the mechanism of dominance of nonsense or frameshift *STAT3* variants. (A)** Schematic diagram of nonsense or frameshift *STAT3* variants found both in our cohort (labeled in red) and in previous studies (labeled in black). **(B and C)** Luciferase assay on *STAT3*$^{-/-}$ A4 cells (B) or HEK293T cells (C) transfected with no vector (mock), EV, WT *STAT3* (WT), or *STAT3* variants, together with the pGL4.47 luciferase reporter construct and an expression vector for *Renilla* luciferase. After 24 h, transfected cells were left untreated or treated with 100 ng/ml sIL-6 for 24 h. The y-axis represents STAT3

transcriptional activity normalized against unstimulated activity in EV-transformed cells. The x-axis indicates the alleles used for transfection. R382W, D427ins17, and Y705F, which have been shown to be amorphic and DN, were used as positive controls. In-house variants are shown in red, previously reported variants in black, and positive controls in blue. **(B)** STAT3 transcriptional activity in *STAT3*$^{-/-}$ A4 cells transfected with mock, EV, WT, or *STAT3* variants (canonical transcripts). STAT3 transcriptional activity in *STAT3*$^{-/-}$ A4 cells transfected with EV was considered to be 0% (red dashed line) and the level of STAT3 transcriptional activity in *STAT3*$^{-/-}$ A4 cells transfected with WT was considered to correspond to 100% activity. The variants are classified on the basis of percentage of STAT3 transcriptional activity as follows: <0%, amorphic; between 0% and 25%, severely hypomorphic; between 25% and 75%, mildly hypomorphic; between 75% and 125%, isomorphic; and >125%, hypermorphic. **(C)** STAT3 transcriptional activity in HEK293T cells expressing endogenous *STAT3* transfected with mock, EV, WT *STAT3* plasmid or various amounts of the *STAT3* variants (described in the upper right box). sIL-6–stimulated EV-transfected HEK293T cells (endogenous *STAT3* activity) are indicated by a red dashed line. The black dashed line represents 50% EV activity. The variants are classified on the basis of endogenous *STAT3* activity; variants with transcription levels below the endogenous level are considered to be DN (weakly DN if >50% activity and strongly DN if <50%), and those with variants above the endogenous level are considered to be not DN. Each experiment (B and C) was independently performed three times. Error bars represent the means with SEM.

We subsequently activated the cells by incubation with IL-6/IL-6Rα (sIL-6) to assess STAT3 transcriptional activity by measuring luciferase activity. Three of the 13 STAT3 cDNA variants (D698Tfs*9, D698Efs*6, and S701Kfs*17) were amorphic (no activity), five (F493Lfs*16, R518*, W562*, Q633*, and Y657*) were severely hypomorphic (between 0% and 25% activity), and another five (R13Vfs*11, Q125*, D371Lfs*14, S381*, and R729Pfs*12) were mildly hypomorphic (between 25% and 75% activity; Fig. 2 B). We then assessed the molecular mechanism of dominance by using each variant allele to transfect human embryonic kidney (HEK) 293T cells, which endogenously express *STAT3*. After transfection with the STAT3-dependent luciferase reporter construct and following sIL-6 stimulation, two variant alleles, R13Vfs*11 and Q125*, were found not to have a DN effect. However, a DN effect was observed for the other 11 variant constructs due to the production of a truncated protein, as described for known DN variants (R382W, D427ins17, and Y705F; Fig. 2 C). Interestingly, R518*, S381*, and D371Lfs*14 also behaved in a DN manner, although the DN effect of these variants appeared to be weaker than that of the other variants. Overall, eight variants had a strong DN effect, five variants had a weaker DN effect, and two had no detectable DN effect (Table S2).

Seven out-of-frame *STAT3* variants create alternative transcripts

The results described above suggested that the mechanism of dominance might depend on the variant. We hypothesized that some variants might generate two or more mRNAs: the canonical transcript and at least one alternative transcript generated by the variant and potentially both LOF and DN. This hypothesis has not been tested for any of the previously reported *STAT3* nonsense or frameshift variants (Abolhassani et al., 2018; Anolik et al., 2009; Natarajan et al., 2018; Renner et al., 2008; Tavassoli et al., 2019; Woellner et al., 2010). We tested the impact of the variants on transcript levels in an exon-trapping assay (Duyk et al., 1990); we tested all HIES-associated *STAT3* nonsense or frameshift variants from our in-house cohort and previous studies (Abolhassani et al., 2018; Anolik et al., 2009; Natarajan et al., 2018; Renner et al., 2008; Tavassoli et al., 2019; Woellner et al., 2010). We first generated variant plasmids for seven nonsense or frameshift variants from our cohort and performed exon trapping (Figs. 3 A and S1 and Table S2). The c.1111_1112del (p.D371Lfs*14), c.1552C>T (p.R518*), and c.1685G>A (p.W562*) variants resulted in the generation of new alternative transcripts. The c.1111_1112del variant encoded a D371Lfs*14 due to the retention of intron 12 as an alternative transcript. The c.1552C>T variant encoded a R518Tfs*14 due to the creation of a new splice donor site. The c.1685G>A variant encoded E552-W562del as an alternative transcript due to the creation of a new splice acceptor site. We then investigated the ratio of these transcripts. For c.1111_1112del, the canonical transcript encoding D371Lfs*14 and the alternative transcript derived from intron retention and encoding D371Lfs*14 were detected at frequencies of 98% and 2%, respectively. For c.1552C>T, the canonical (R518*) and alternative (R518Tfs*14) transcripts were detected at frequencies of 80% and 20%, respectively. For c.1685G>A, the canonical (W562*) and alternative (E552-W562del) transcripts were present at frequencies of 83% and 17%, respectively. The other variants did not generate any detectable alternative transcripts (Table S2). We then investigated alternative splicing for the eight previously reported nonsense or frameshift variants pLOF (Natarajan et al., 2018; Tavassoli et al., 2019; Figs. 3 A and S1 and Table S2). Next, we performed RNA sequencing (RNA-seq) to detect *STAT3* alternative transcripts in the patient's heterozygous cells. RNA-seq data from P3's EBV-B cells, two controls' EBV-B cells, and a patient's with a deep intronic mutation creating a new splice site (Khourieh et al., 2019) suggested that the c.1552C>T (p.R518*) mutation led to a new event in the vicinity of the mutation, but we failed to identify alternative transcripts due to low coverage (Fig. S2 A). We thus performed a deep sequencing of preamplified *STAT3* cDNA from P3's, P4's, and two controls' primary fibroblasts pretreated with emetine dihydrochloride hydrate, an inhibitor of mRNA decay process (Noensie and Dietz, 2001). These analyses revealed that the patients' cells (P3, P4) actually display *STAT3* alternative transcripts, consistent with the results of exon-trapping (Fig. 3 B; and Fig. S2, A–C). These analyses also revealed that P3's cells harbored a new *STAT3* alternative transcript (deletion of exon 17–19; p.N489Vfs*8), which was not detected by exon-trapping (Fig. 3 B). We found that c.1140-2A>C, c.1140-2A>G, c.1140-3C>G (p.S381*), and c.2144+1G>A (p.S701Kfs*17) resulted in alternative transcripts. Indeed, c.1140-2A>C, c.1140-2A>G, and c.1140-3C>G created S381Pfs*2, and c.2144+1G>A created S701-D732delinsN as alternative transcripts. For c.1140-2A>C, S381* had a frequency of 52% and S381Pfs*2 had a frequency of 48%. For c.1140-2A>G, S381* had a frequency of 81% and S381Pfs*2 had a frequency of 19%. By contrast, for c.1140-3C>G, S381* had a frequency of 0% and S381Pfs*2 had a frequency of 100%. According to published

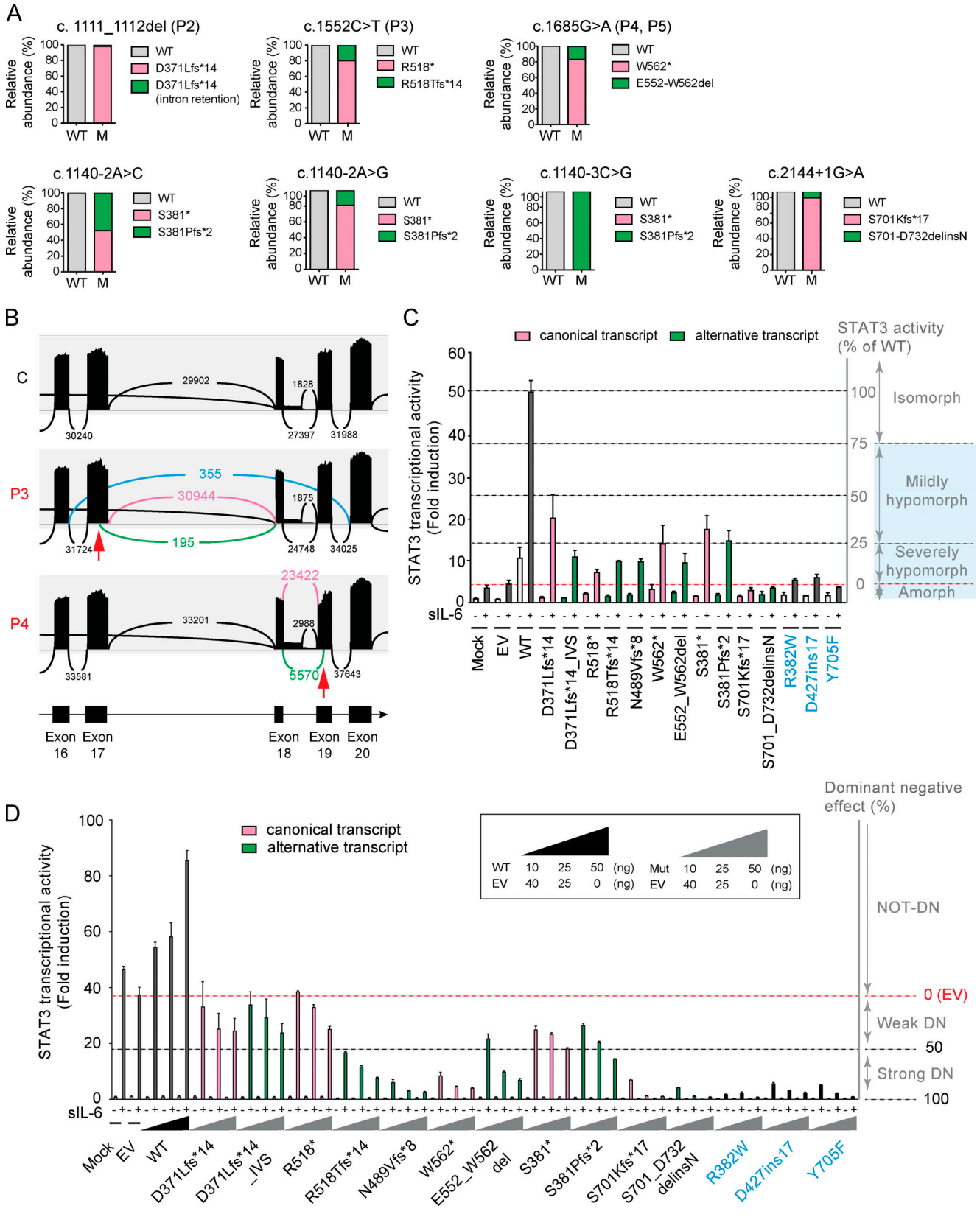

Figure 3. **Identification and characterization of abnormal splicing in *STAT3* nonsense or frameshift variants in HIES. (A)** The ratio of canonical transcripts to alternative transcripts was determined by exon trapping. The percentages of WT (gray) and splice variants (canonical transcript in pink and alternative transcripts in green) of *STAT3* transcripts are shown for nonsense or frameshift variants. M, mutant. **(B)** Deep RNA analysis for the identification of new alternative splicing in HIES patients' primary fibroblasts with *STAT3* nonsense variants (P3 and P4). Amplified *STAT3* cDNA were analyzed by MiSeq to identify the rare splicing events and shown by Sashimi plot representation using Integrative Genomics Viewer. Pink colored lines and legends represent

canonical splicing. Green colored lines and legends represents alternative splicing already detected in the exon-trapping assay. Blue colored lines and legends represent alternative splicing newly identified in this assay. C, healthy control; P3, R518*; P4, W562*. Red arrow represents the position of each variant. **(C and D)** STAT3 transcriptional activity in *STAT3*$^{-/-}$ A4 cells (C) or HEK293T cells (D) transfected with mock, EV, WT, or *STAT3* variants, including variants generating alternative transcripts, together with the pGL4.47 reporter construct and an expression vector for *Renilla* luciferase. After 24 h, the transfected cells were left untreated or treated with 100 ng/ml sIL-6 for 24 h. The y-axis represents STAT3 transcriptional activity levels normalized against unstimulated activity in EV-transformed cells. The x-axis indicates the alleles used for transfection. R382W, D427ins17, and Y705F were used as positive controls. The pink bar represents the canonical transcript and the green bar represents the alternative transcript. Stimulated EV-transfected HEK293T cell activity is indicated by a red dashed line. All variants are classified according to the rules described in Fig. 2, B and C. Each luciferase assay (C and D) was independently performed three times. Error bars represent the means with SEM.

reports, c.1140-3C>G generates S381*, resulting in HI (Natarajan et al., 2018), but we were unable to detect this transcript in our analysis. For c.2144+1G>A, S701Kfs*17 had a frequency of 92% and S701-D732delinsN had a frequency of 8%. The other variants produced the canonical transcripts only (Table S2).

The eight alternative transcripts encode STAT3 proteins that are DN

We measured protein levels with mAbs directed against the C-terminal part of STAT3 in overexpression assays in *STAT3*$^{-/-}$ A4 cells. All the new alternative transcripts identified by exon-trapping were produced as expected (Fig. S3, A and B; and Table S2). We assessed the allele activity of each of the alternative transcripts by transfecting *STAT3*$^{-/-}$ A4 cells with each variant allele. We found that one of the variants was amorphic (S701-D732delinsN), four were severely hypomorphic (D371Lfs*14, N489Vfs*8, R518Tfs*14, E552-W562del), and one was mildly hypomorphic (S381Pfs*2; Fig. 3 C and Table S2). We assessed the mechanism of dominance of these six alternative transcripts by transfecting HEK293T cells, which endogenously express *STAT3*, with each of the variant alleles. We found that the variant alleles behaved in a DN manner (Fig. 3 D and Table S2). All variants with canonical transcripts displaying weak negative dominance in the previous experiments (Fig. 2 B) generated alternative transcripts with DN effects. Interestingly, R518Tfs*14 and S381Pfs*2 had stronger DN effects than their canonical transcripts (Fig. 3 D). In addition, the N489Vfs*8 rare alternative transcript that was identified in R518* patient's cells had a strong DN effect (Fig. 3 D). In cotransfection experiments with the canonical and their alternative variant cDNAs used in the ratios determined in exon-trapping experiments, the coexpressed variant alleles did indeed behave in a DN manner in terms of STAT3 transcriptional activity (Fig. S3 C). 13 of 15 *STAT3* alleles pLOF encoded a canonical isoform (n = 13) or a new isoform encoded by an alternative transcript (n = 8) that was hypomorphic (n = 7) or LOF (n = 1) and had a DN effect.

Two out-of-frame alleles are DN by as they reinitiate translation

We studied the two remaining variant alleles, R13Vfs*11 and Q125*, for which the canonical transcripts were not DN, and which did not express alternative transcripts. We considered the possibility of a reinitiation of translation in R13Vfs*11 and Q125*, because immunoblots revealed the presence of proteins with a lower molecular weight (Fig. S3 A). We first determined which Met after each premature stop codon was used for reinitiation. We mutated each Met codon to a Leu or Ala codon and used the mutant constructs to transfect *STAT3*$^{-/-}$ A4 cells, in which we checked protein levels to determine whether translation reinitiation had occurred (Fig. 4 A). For the R13Vfs*11 allele, we identified two main reinitiation sites, one at position 28 and the other at position 99 (Fig. 4 A). For Q125*, the same approach identified two reinitiation sites, Met143 and Met162 (Fig. 4 A). We then measured the STAT3 activity conferred by these cDNAs. For each R13Vfs*11 and Q125* variant, we constructed three additional plasmids: one with the premature stop encoding a truncated short form without a reinitiation transcript (R13Vfs*11 and Q125*), a second with the first reinitiation transcript only (Met28 and Met143), and a third with the second reinitiation transcript only (Met99 and Met162; Fig. 4 B). The truncated R13Vfs*11 form with the premature stop codon resulted in a loss of STAT3 activity through negative dominance, whereas both reinitiation constructs were either isomorphic or slightly hypermorphic (Fig. 4 C). The truncated form of the Q125* construct was also LOF and DN. Moreover, the Met143 construct behaved in a hypermorphic, but not DN, manner, whereas the Met162 reinitiation construct was both amorphic and DN (Fig. 4 C). These findings are consistent with previous reports that amino acids 150–162 in the coiled-coil domain (CCD) were indispensable for the nuclear translocation of STAT3 (Liu et al., 2005). Thus, both the R13Vfs* and Q125* variants can underlie the reinitiation of translation, with the encoded proteins having a DN effect on STAT3 transcriptional activity. All the out-of-frame variants of STAT3 were DN but by different mechanisms involving truncated proteins (n = 6), isoforms from alternative transcripts (n = 1), proteins generated through translation reinitiation (n = 2), or combinations of these mechanisms (n = 6).

Activity and mechanism of dominance in all *STAT3* variants reported in AD-HIES patients

In the Human Gene Mutation Database of pathological variants and PubMed, 143 variants are identified as causal variants of AD-HIES (Fig. S3 and Table S3; Abolhassani et al., 2018; Al Khatib et al., 2009; Alcántara-Montiel et al., 2016; Anolik et al., 2009; Avery et al., 2010; Egawa et al., 2019; Eken et al., 2020; Felgentreff et al., 2014; Freeman et al., 2013; Giacomelli et al., 2011; Hagl et al., 2016; He et al., 2012; Heimall et al., 2011; Holland et al., 2007; Jiao et al., 2008; Khourieh et al., 2019; Kim et al., 2009; Kumánovics et al., 2010; Larsen et al., 2019; Ma et al., 2012; Ma et al., 2008; Merli et al., 2014; Minegishi et al., 2009; Minegishi et al., 2007; Miyazaki et al., 2011; Moens et al., 2017; Moens et al., 2014; Mogensen, 2013; Natarajan et al., 2018; Papanastasiou et al., 2010; Pelham et al., 2016; Powers et al.,

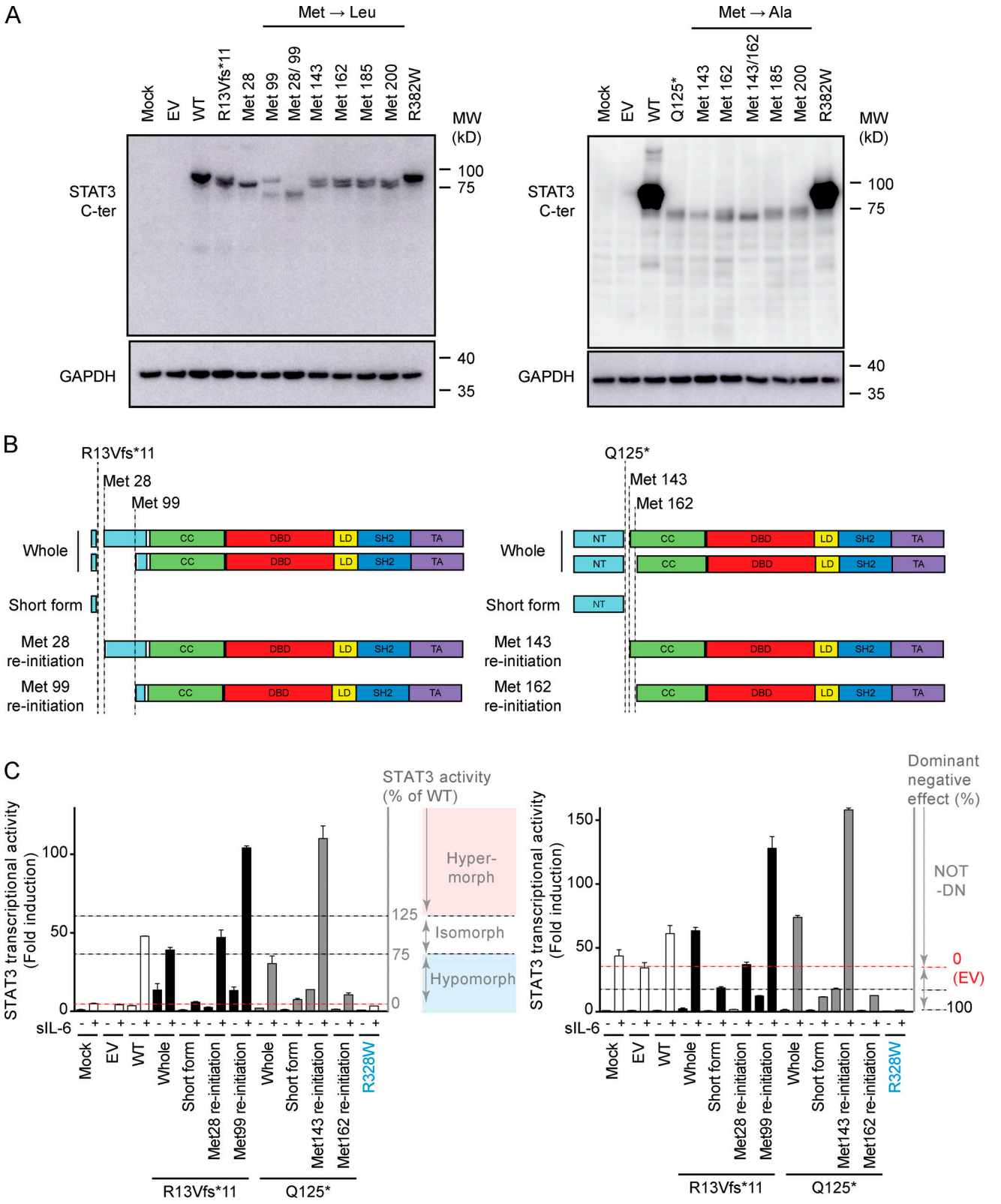

Figure 4. **Analysis of translation reinitiation for the R13Vfs*11 and Q125* variants of *STAT3*. (A)** Western blot of extracts from nontransfected *STAT3*$^{-/-}$ A4 cells (mock), A4 cells transfected with EV, the *STAT3* WT allele, or the *STAT3* variant allele of interest. All extracts were probed with an antibody against the C terminus (C-ter) of the STAT3 protein. (Left) Each Met codon after the premature stop codon was mutated to give a Leu codon, at Met28, Met99, Met143, Met162, Met185, and Met200. Variants with such mutations at both Met28 and Met99 were also constructed. R13Vfs*11 and each variant with a mutated Met codon were used to transfect A4 cells, and the STAT3 protein profile was then checked. Right: Using the same procedure as for R13Vfs*11, each Met codon after the premature stop codon was mutated to give an Ala codon at Met143, Met162, Met185, and Met200. A construct with a double Met143Ala and

Met162Ala mutation was also constructed. Q125* and each mutated construct was used to transfect *STAT3*-null A4 cells, and STAT3 protein levels were then checked. MW, molecular weight. **(B)** A short-form construct with a premature stop codon (R13Vfs*11 and Q125*) and a reinitiation construct (translation starts at Met28, Met99, Met143, and Met162) were designed and constructed from each variant plasmid by mutagenesis. CC, coiled-coil domain; DBD, DNA-binding domain; LD, linker domain; TA, transactivation domain. **(C)** Luciferase assay on *STAT3*$^{-/-}$ A4 cells (left figure) or HEK293T cells (right figure) transfected with mock, EV, WT, or *STAT3* variants, including variants generating alternative transcripts, together with the pGL4.47 reporter construct and an expression vector for *Renilla* luciferase. After 24 h, the transfected cells were left untreated or treated with 100 ng/ml sIL-6 for 24 h. The y-axis represents STAT3 transcriptional activity normalized against unstimulated activity in EV-transformed cells. The x-axis shows the alleles used for transfection. R382W was used as a positive control for the DN effect. The black bar represents the results for the R13Vfs*11 variant, and the gray bar represents the results for the Q125* variant. The red dashed line represents activity in stimulated EV-transformed cells. All variants are classified according to the rules described in Fig. 2, B and C. Each experiment (A and C) was independently performed three times. Error bars represent the means with SEM.

2009; Renner et al., 2008; Renner et al., 2007; Robinson et al., 2011b; Schimke et al., 2010; Sundin et al., 2014; van de Veerdonk et al., 2010; Vinh et al., 2010; Woellner et al., 2010; Wolach et al., 2014; Wu et al., 2017; Zhang et al., 2013). In summary, 114 of these variants are missense variants, 21 are in-frame indels, and 8 are out-of-frame variants. Among the 143 reported variants, 2% (n = 3) concern the N-terminal domain, 43% (n = 62) the DNA-binding domain, 5% (n = 7) the linker domain, 35% (n = 50) the SH2 domain (SH2), and 15% (n = 21) the transactivation domain (Fig. S4 and Table S4). There were no reported variants of the CCD in patients with HIES (Fig. S4 and Table S4), whereas seven variants of the CCD have been reported for STAT3 gain-of-function syndrome (Fabre et al., 2019). We assessed the allele activity and mechanism of dominance for all these variants in our luciferase assay system. We found that 107 of the 114 missense variants were amorphic or hypomorphic, 5 were isomorphic, and 2 were hypermorphic (Fig. 5 A and Table S3). Strong DN effects (>50%) were observed for 95 variants, whereas the DN effect was not convincingly strong for 19 variants (Fig. 5 B and Table S3). All 21 in-frame indels were amorphic or hypomorphic, and 20 of them displayed strong DN effects; only one variant (c.1107_1109del (p.D369_L370delinsE)) had a DN effect that was not convincingly strong (Fig. 5, A and B; and Table S3). We then analyzed more precisely the mechanism of dominance for the 20 variants without strong DN effects in luciferase assays (weak DN, 9; not DN, 11). We found that five had dose-dependent DN effects (F384C, D369_L370delinsE, R423Q, N472D, and K642E; Fig. S5 A). We considered these variants to be DN, because dose dependence is an element of the definition of negative dominance. The remaining 15 variants had no detectable dose-dependent DN effects, although some did exert mild DN effects (Fig. S5 A and Table S5). We investigated whether the variants generated alternative transcripts encoding proteins with DN effects using exon-trapping assays, as in the previous experiment. 13 of the 15 variants generated alternative transcripts (Table S5), and 8 of these alternative transcripts had DN effects (Fig. S5, B and C; and Table S5). The remaining seven variants did not appear to be DN (H58Y, R84Q, H332R, R335W, T341N, N425Y, and A744V). The corresponding patients may benefit from (1) being reanalyzed genetically, as they might carry mutations in other HIES-causing genes (e.g., *IL6ST*, *ZNF341*, and *IL6R*) or (2) being analyzed more thoroughly for STAT3 mRNAs using primary cells, as our exon-trapping may have missed an alternative transcript (Alcántara-Montiel et al., 2016; Freeman et al., 2013; Jabara et al., 2012; Miyazaki et al., 2011; Renner et al., 2008; Woellner et al., 2010). Thus, some missense variants can influence splicing, generating aberrant transcripts and resulting in DN effects. We found that 95% (136 variants) of the 143 variants behaved in a DN manner at the cellular level (Fig. 6; Table S3 and Table S5), either directly or through the production of aberrant transcripts.

Activity and mechanism of dominance of 14 *STAT3* variants reported in gnomAD

We investigated a subset of *STAT3* variants found in the general population. The gnomAD database includes 1,095 *STAT3* variants, of which 141 are missense, 1 is an in-frame deletion, 1 is a nonsense variant, and 167 are synonymous. We selected 14 gnomAD variants, including 12 missense variants (Q125E, R246Q, A376V, G402S, D427G, V461L, I498V, R518Q, A702T, G743V, S763L, and A766T) with either a minor allele frequency above 1×10^{-4} or a CADD score higher than 30, 1 variant (E239del) with an in-frame deletion, and the only variant pLOF (Q247*; minor allele frequency, 4×10^{-6}; CADD, 39; Fig. 7 A and Table S6). We assessed their allele activity and the mechanism of dominance in the same luciferase assay system. Only Q247* was severely hypomorphic, three variants (Q125E, D427, and G743V) were mildly hypomorphic, and two variants (A376V and R518Q) were hypermorphic, whereas the remaining eight variants had normal activity (Fig. 7 B). None of the 14 gnomAD variants were found to be DN (Fig. 7 C). The sole LOF variant (Q247*) had no DN effect, even when the amount of the Q247* allele was increased (Fig. 7 D). We also showed that this variant did not create a splice site or reinitiate translation (Fig. 7, E and F). It was not possible to retrieve clinical data for the carrier of this mutation, but this individual belonged to a neurocohort from gnomAD and was unlikely to have HIES. Thus, the analysis of *STAT3* variants in the general population suggested that most of the common variants are isomorphic and that the only variant predicted to be LOF was indeed LOF but did not display DN behavior, suggesting that *STAT3* HI is clinically silent.

Allele activity and prediction of the functional impact of *STAT3* variants

An analysis of 150 heterozygous *STAT3* variants in AD-*STAT3*-HIES (143 already reported and 7 new variants reported here), with software for predicting the deleteriousness of mutations (Kircher et al., 2014) identified only one deep intronic variant leading to alternative splicing (Khourieh et al., 2019), which was predicted to be nonpathogenic, with a low CADD score (8.742), below the 99% confidence threshold MSC score for *STAT3* (16.4; Itan et al., 2016; Rentzsch et al., 2019; Zhang et al., 2018a). All the

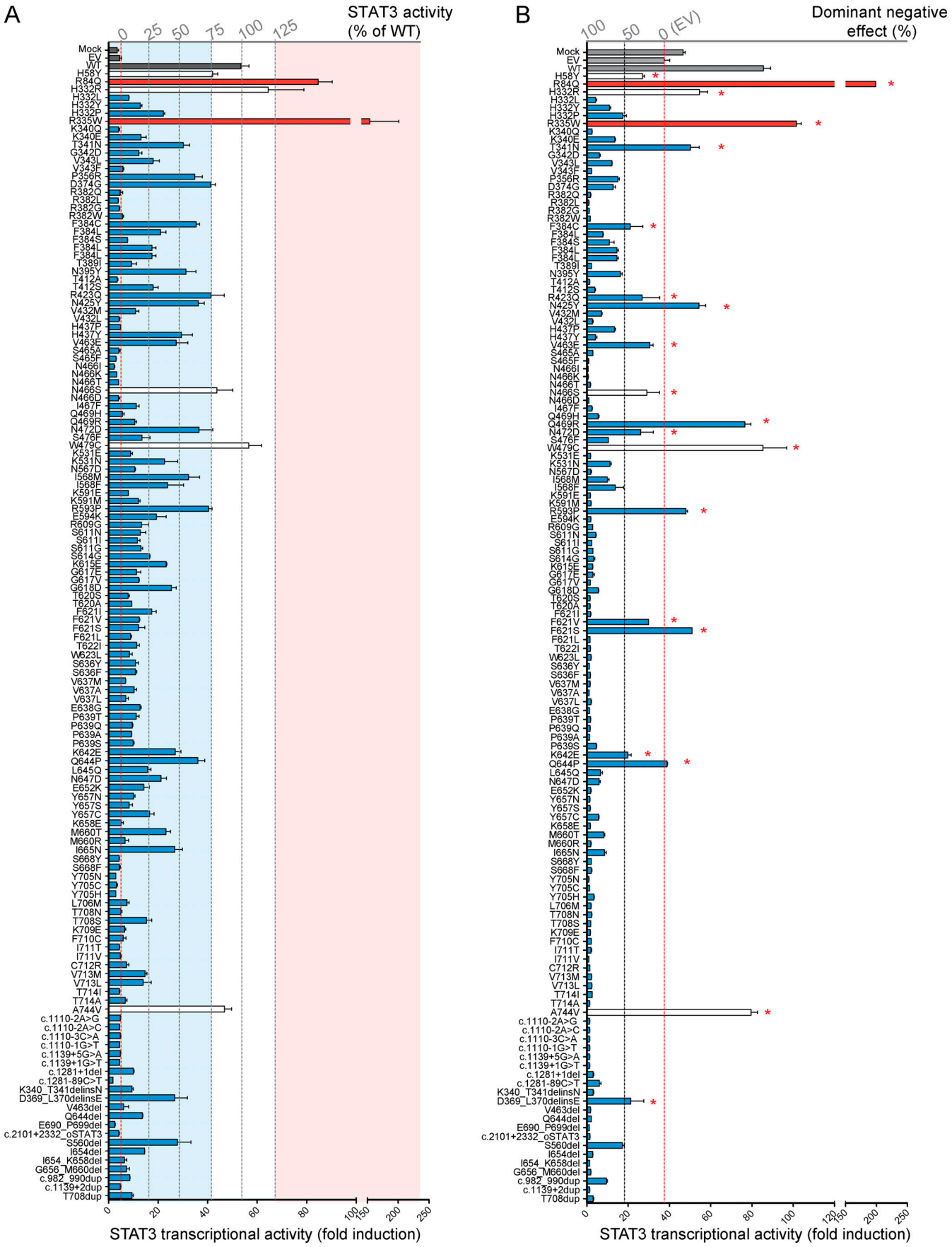

Figure 5. **Allele activity and the mechanism of dominance for all reported *STAT3* variants in AD-STAT3-HIES.** Luciferase assay on *STAT3*$^{-/-}$ A4 cells (A) or HEK293T cells (B) transfected with mock, EV, WT, or the reported *STAT3* variants, together with the pGL4.47 reporter construct and an expression vector for *Renilla* luciferase. After 24 h, the transfected cells were left untreated or treated with 100 ng/ml sIL-6 for 24 h. In A and B, only STAT3 transcriptional activity following sIL-6 stimulation is shown. All variants are classified according to the rules described in Fig. 2, B and C. **(A)** The red bar represents hypermorphic variants, the white bar represents isomorphic variants, and the blue bar represents amorphic or hypomorphic variants. **(B)** The color of the bars corresponds to the description in A. The 20 variants associated with an asterisk were considered to be not DN in this analysis (both not-DN and weak-DN variants were assigned to this category here). All variants are classified according to the rules described in Fig. 2, B and C. Each experiment (A and B) was independently performed twice. Error bars represent the means with SEM.

remaining 149 variants were predicted to be deleterious (CADD >16.4; Table S3). By contrast, 99% (141/143) of the 143 heterozygous nonsynonymous coding variants of *STAT3* in the gnomAD database (missense, 141; in-frame deletion, 1; nonsense, 1) had CADD scores above the MSC, suggesting that they may be deleterious (Fig. 7 A). We analyzed the correlation between CADD and STAT3 activity for all the variants tested. There was no correlation between STAT3 activity and CADD score (R^2 = 0.013). Five variants (3.3%) identified as isomorphic by our assay were predicted to be deleterious by CADD and may therefore be considered false positives (FPs). By contrast, all the hypomorphic or amorphic variants were predicted to be deleterious and are therefore true positives (Fig. 8 A). We also tested the performance of other software for predicting the deleteriousness of mutations (Condel, PPH2, Sift, FATHMM, Mutation Assessor, and Provean; Adzhubei et al., 2010; Choi and Chan, 2015; González-Pérez and López-Bigas, 2011; Reva et al., 2011; Rogers et al., 2018; Vaser et al., 2016). For all six programs, there was no correlation between the predicted deleteriousness score and the activity of the *STAT3* variants (Fig. 8 B). Thus, predictions of

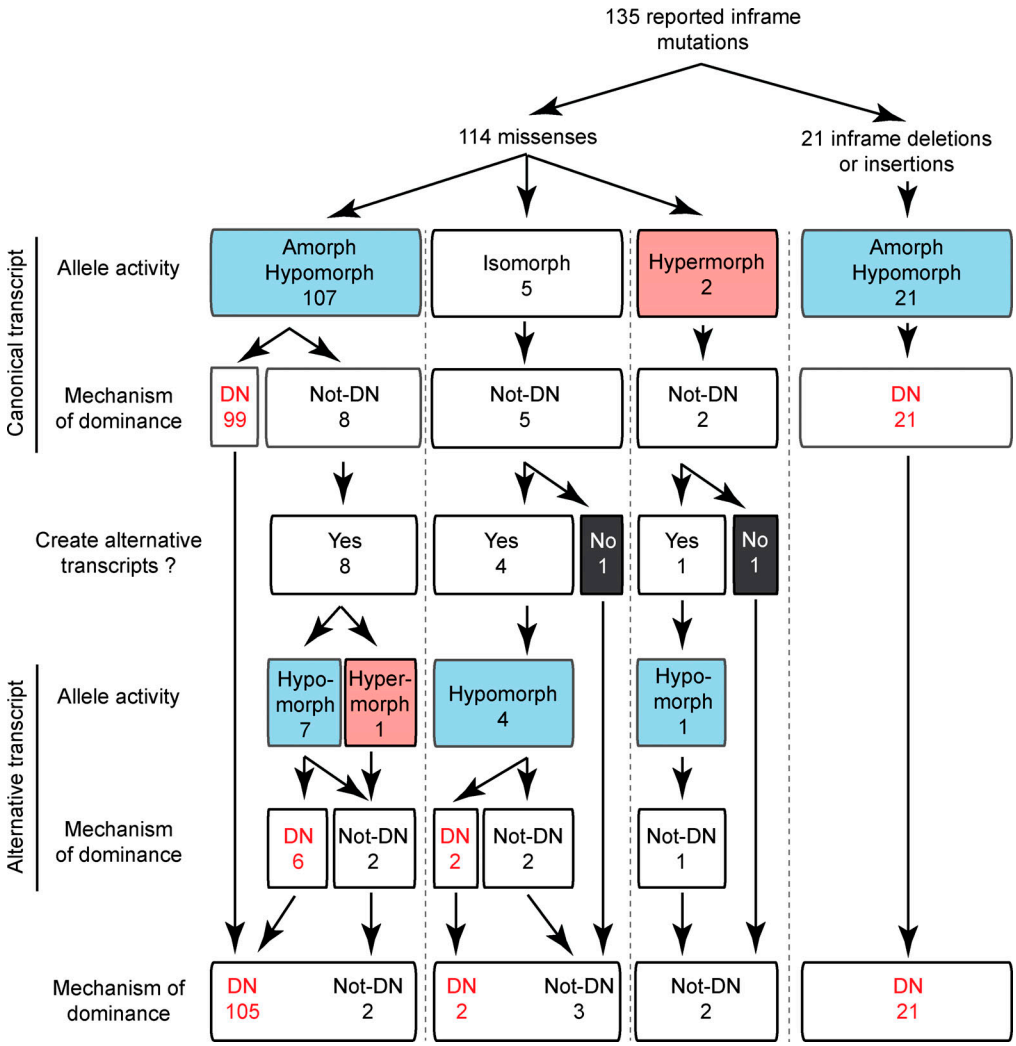

Figure 6. **Schematic summary of the analysis for all reported in-frame *STAT3* variants in AD-STAT3-HIES.** Schematic representation of the results (allele activity and mechanism of dominance) for the 135 in-frame *STAT3* variants analyzed.

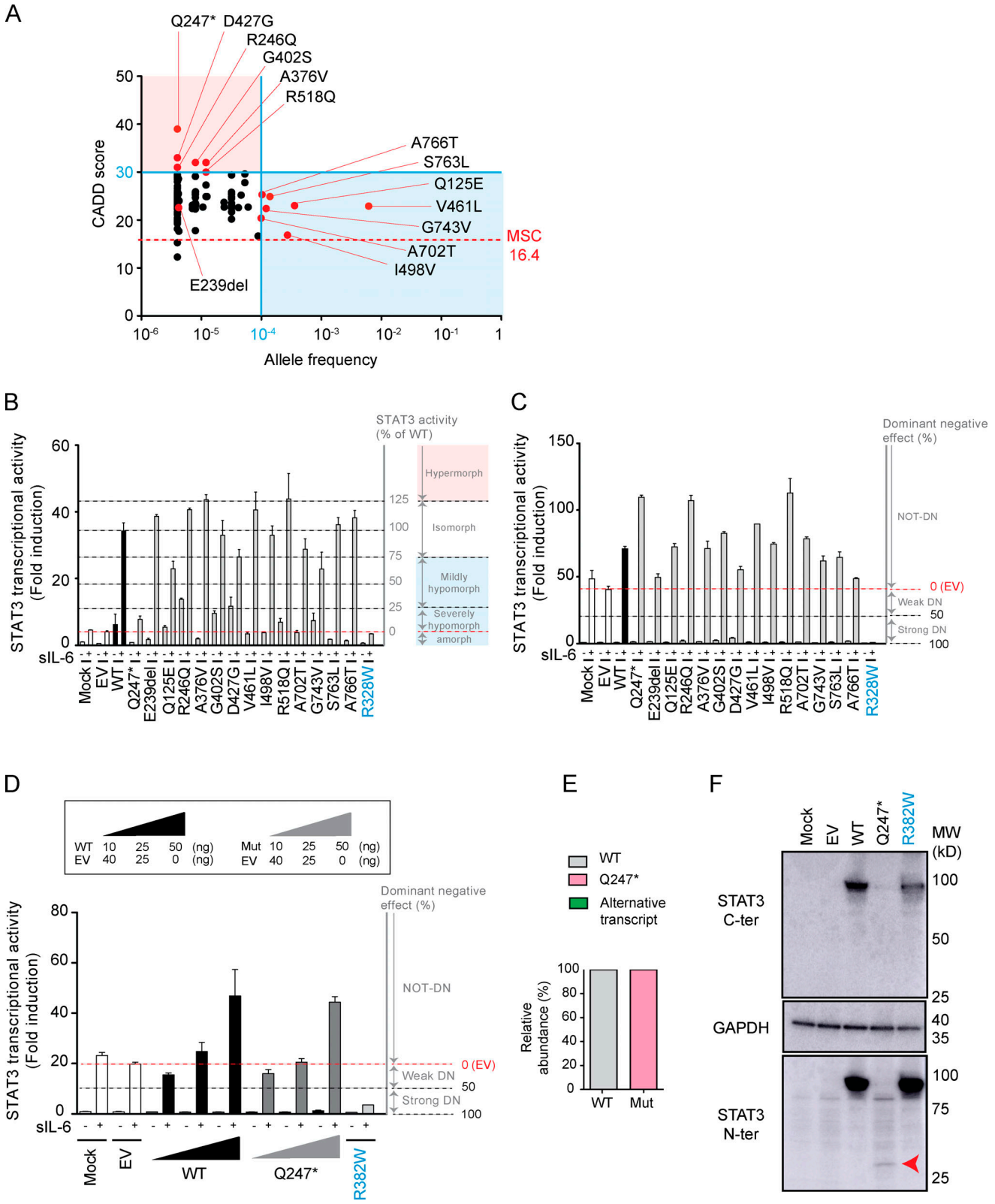

Figure 7. **Allele activity and the mechanism of dominance for *STAT3* variants found in the general population. (A)** Graph showing the predicted CADD scores and global allele frequencies of nonsynonymous coding *STAT3* variants found in gnomAD (v2.1). 14 variants, including a nonsense variant, were selected and analyzed (shown in red). The CADD-MSC score (99% confidence interval) for STAT3 is indicated by a red dashed line. **(B and C)** Luciferase assay on *STAT3*$^{-/-}$ A4 cells (B) or HEK293T cells (C) transfected with mock, EV, WT, or *STAT3* variants from gnomAD, together with the pGL4.47 reporter construct and an expression vector for *Renilla* luciferase. After 24 h, the transfected cells were left untreated or treated with 100 ng/ml sIL-6 for 24 h. The y-axis represents STAT3 transcriptional activity normalized against unstimulated activity in EV-transformed cells. The x-paraxis represents the alleles used for transfection.

R382W was used as a positive control, as its functional impact has already been determined. **(D)** Luciferase assay on HEK293T cells, which have endogenous *STAT3*, with various amounts of WT or Q247*. **(E)** Schematic representation of the ratio of canonical to alternative transcripts, according to an exon-trapping assay on the Q247* variant. Exon-trapping analysis revealed that all the transcripts were canonical (represented in pink), with none resulting in alternative transcripts, for the Q247* variant. **(F)** Western blot of extracts from nontransfected *STAT3*$^{-/-}$ A4 cells (mock), A4 cells transfected with pCMV6 EV, the *STAT3* WT allele, or the *STAT3* variant alleles (Q247*). All extracts were probed with mAbs specific for the C-terminal part of STAT3 or the N-terminal part of the STAT3 protein. No protein was detected with an antibody recognizing the C terminus, whereas a faint band at ∼25 kD (red arrow) was detected with an antibody recognizing the N terminus, suggesting that the N-terminal part (1–246) of STAT3 is weakly expressed. Each experiment (B, C, D, and F) was independently performed twice. Error bars represent the means with SEM.

deleteriousness do not provide an adequate estimate of the experimentally determined deleteriousness of the variants and, by inference, their pathogenicity.

The population genetics of human *STAT3* supports a mechanism of negative dominance

Biologically disruptive heterozygous variants of *STAT3* are likely to have clinical effects. Consistently, the gene damage index for *STAT3* is low (1.5; Itan et al., 2015). Human genetic variants that cause severe diseases are progressively purged from the population, as their carriers have fewer children than noncarriers. Indeed, *STAT3* is under strong purifying selection, with an *f* value of 0.26 (among the top 2% of human protein genes in terms of constraint; Table S7; Eilertson et al., 2012). This natural process, negative selection, has a stronger effect on disease variants that affects heterozygous individuals (Fuller et al., 2019). We recently developed a new statistical tool, called consensus negative selection (CoNeS), combining interspecies and intraspecies measurements of negative selection, with which we showed that genes underlying AD or X-linked IEI are under stronger negative selection than those underlying AR IEI (Rapaport et al., 2021). In this system, as expected, *STAT3* was found to be under very strong negative selection, with a CoNeS value of −1.94 (Fig. 8 C and Table S7). Only three genes underlying IEI have been shown to be under stronger negative selection (*ACTB*, −2.17; *CHD7*, −2.11; and *KMT2D*, −2.75; Table S7). This finding is consistent with the AD inheritance of *STAT3*-HIES and the low frequency of missense variants in the general population, as shown by our analysis of the gnomAD database. Moreover, there is only one nonsense variant in gnomAD (Q247*) pLOF, but this variant is not DN (Fig. 7, B–D). In our analysis of 150 *STAT3* variants, 143 (95%) were predicted to be DN, causing HIES (Table S3). Thus, the population genetics of *STAT3* provides no evidence for HI associated with AD disease in *STAT3*.

Discussion

Following the discovery of the first genetic etiologies of HIES (heterozygous variants of *STAT3*; Minegishi et al., 2007) in 2007, 143 private *STAT3* variants had been reported in HIES patients by July 1, 2020 (and 7 others are reported here). However, STAT3 activity and the mechanism of dominance have been experimentally elucidated for only six variants (Khourieh et al., 2019; Minegishi et al., 2007). We show here that the canonical transcripts of 95.3% (143/150) of these variants encode STAT3 proteins with little or no STAT3 activity. 15 of these variants were pLOF. All but one variant associated with HIES had a CADD scores above the MSC (16.4), predictive of deleteriousness, resulting in a very low false-negative (FN) rate, at 0.7% (1/150). The only incorrectly predicted variant is actually a deep intronic variant, with a CADD of 8.742. Misprediction for intronic variants is a well-known source of FNs (Mather et al., 2016). Conversely, five variants from HIES patients predicted to be deleterious actually encoded STAT3 proteins with normal activity, resulting in a FP rate of 3.3%. The remaining two have a lower CADD score. With the benefit of hindsight, the patients carrying the seven isomorphic variants did not have HIES or had not been studied for other genetic etiologies. By contrast, only one of the coding variants from the gnomAD database selected for experimental testing on the basis of their rarity and high CADD score (n = 14), a nonsense variant (pLOF), was experimentally LOF, and none of these variants were DN (including the LOF variant). We did not thoroughly investigate all other 143 nonsynonymous coding variants found in the general population, but we can assume that most public variants are isomorphic, and at least not DN, because they are more common or have lower CADD scores than those tested. Moreover, the gnomAD database includes very few patients with developmental or infectious diseases, the two major characteristic of individuals with HIES. Nevertheless, most of the nonsynonymous coding variants found in the general population were predicted to be deleterious on the basis of CADD, with a FP rate of 98% that questions the usefulness of this score to diagnose HIES patients (141/143; Fig. 8 A). Further experimental studies are required to determine whether these predictions are correct or false. Meanwhile, computational prediction of the functional impact of coding variants of *STAT3* remains challenging due to the high FP rate. We therefore suggest that any new variant found in a patient with HIES should be tested functionally for an accurate molecular diagnosis.

The mechanism of dominance underlying AD conditions should, ideally, be reliably established, to improve both our understanding of the pathogenesis of the condition and its clinical management. Before the identification of nonsense variants in HIES patients, most studies referred to the original 2007 paper and did not call the mechanism of negative dominance for HIES into question. By experimentally testing 150 *STAT3* variants found in HIES patients, we show that AD STAT3 deficiency invariably underlies HIES by DN. HIES-causing *STAT3* variants encode (1) truncated proteins, (2) neoproteins generated from a translation reinitiation codon, (3) isoforms from alternative transcripts, or a combination thereof, which account for their DN. These findings suggest that variants of uncertain significance in *STAT3* or other genes can benefit from being experimentally tested at the transcript level by exon

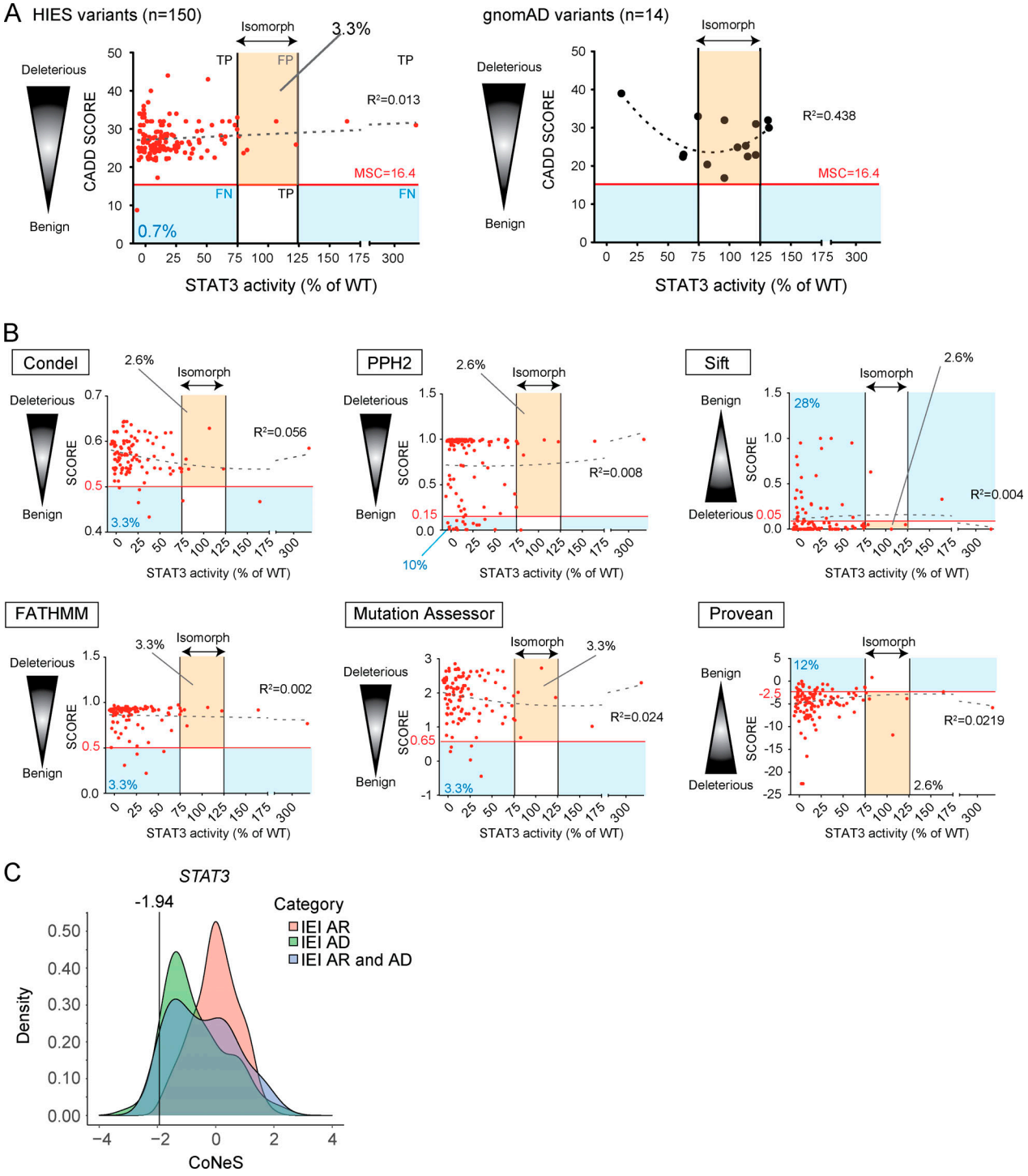

Figure 8. **Population and evolutionary genetics for human *STAT3*. (A)** Diagram showing the correlation between predicted CADD scores and percentage of STAT3 transcriptional activity for all 150 *STAT3* variants (canonical transcripts; red circles, left figure) and 14 gnomAD variants (black circles, right figure) analyzed here. The y-axis represents the CADD score, and the x-axis represents the percentage of STAT3 transcriptional activity. The STAT3 transcriptional activity of all variants was normalized against WT STAT3 transcriptional activity. The CADD-MSC score (99% confidence interval) for STAT3 is indicated by a red solid line. The gray dashed line is the regression line (R^2). The blue rectangle represents the FN area, and the yellow rectangle represents the FP area. The white rectangle represents the true-positive (TP) area. **(B)** We used six programs other than CADD (Condel, FATHMM, Mutation Assessor, Polyphen2 [PPH2], Provean, and Sift) to predict the impact of the *STAT3* variants (canonical transcripts), and we compared the scores obtained with transcription levels. In each diagram, the red solid line represents the mutational cutoff value. The blue rectangle represents the FN area, and the pale orange rectangle represents the FP area. The gray dashed line is the regression line (R^2). **(C)** CoNeS analysis. CoNeS is our custom-built score integrating known negative selection scores through a principal-component projection. The mean value is 0, and low values (negative values) correspond to strong negative selection.

trapping and/or deep RNA-seq (Boisson et al., 2019). In terms of population genetics, *STAT3* is under strong purifying selection (Rapaport et al., 2021), consistent with the reported AD mode of inheritance. Interestingly, in the absence of a pLOF allele in public databases (with one exception), *STAT3* clusters with other genes (Table S7) for which AD phenotypes have been shown to be due to HI (Lek et al., 2016). Our work suggests an alternative hypothesis: pLOF variants are absent from public databases because these alleles are expressed and have a DN effect on the WT allele. Our finding that the only nonsense variant (pLOF) in gnomAD (assuming that the person does not have a HIES phenotype) was actually amorphic, but not DN, is consistent with this alternative hypothesis. It is also consistent with the absence of reports of a phenotype similar to HIES in mice heterozygous for a null loss-of-expression *Stat3* allele, whereas a DN mouse model (expressing the DN V463del allele) reproduces some of the features of HIES patients (Hillmer et al., 2016; Panopoulos et al., 2006; Siegel et al., 2013; Steward-Tharp et al., 2014; Zhang et al., 2010a; Zhang et al., 2018b). In addition, to our knowledge, incomplete penetrance has not been reported for AD-*STAT3*-HIES, whereas it is frequently reported in cases of dominance by HI (Bolze et al., 2018; Borghini et al., 2011; Rieux-Laucat and Casanova, 2014). Overall, our work provides an overarching view of *STAT3* variants in patients with HIES and the general population and establishes that negative dominance is the only mechanism of dominance underlying AD-HIES in patients heterozygous for pathogenic *STAT3* variants.

Materials and methods

Case reports

P1 (kindred A) is a 16-yr-old boy of Syrian origin. He was born at full term to consanguineous parents. He had a history of recurrent sinopulmonary infections during childhood, with failure to thrive (weight and height below the third percentile for age). He developed right lobar pneumonia and bronchiectasis. Bronchoalveolar lavage fluid culture yielded *Aspergillus flavus*. Mycobacteria were not detected (TB culture, PCR, and cultures of acid-alcohol–resistant bacilli were negative). P1 was diagnosed with invasive pulmonary aspergillosis, leading to the initiation of treatment with itraconazole and methylprednisolone. He was admitted to hospital while on treatment for invasive aspergillosis in the lung. He also had a large abscess in the left frontal lobe of the brain and the left lobe of the cerebellum. Culture of a brain biopsy specimen also yielded *A. flavus*. Laboratory tests revealed a neutrophil count of 1,700/mm^3, a lymphocyte count of 1,300/mm^3, a monocyte count of 400/mm^3, and an eosinophil count of 1,700/mm^3. Serum Ig levels were 2,180 mg/dl for IgG, 130 mg/dl for IgM, 1,119 mg/dl for IgA, and 7,430 IU/ml for IgE. The patient's IgE level was quite high, and he had an NIH score of 42 but no skin abscesses, primary tooth retention, scoliosis, bone fractures, candidiasis, eczema, rash, or characteristic facial features. HIES was suspected, and a genetic study was conducted. At the age of 14 yr, a heterozygous nonsense variant, c.373C>T, of *STAT3* was identified by whole-exome sequencing (WES) and confirmed by Sanger sequencing. The patient was therefore diagnosed with AD-*STAT3*-HIES. This variant was not identified in his parents, suggesting that it was a de novo variant. The brain and cerebellum lesions regressed on treatment with amphotericin B, voriconazole, caspofungin, and G-CSF. The patient is currently receiving voriconazole prophylaxis and Ig replacement therapy.

P2 (kindred B) is a 37-yr-old man of Australian origin. His mother died at the age of 20 yr from pneumonia (no other details were available). His sister and his two young children are all healthy. From childhood, P2 suffered from an inflammatory skin disease (labeled as psoriasis), but with no obvious history of pyogenic skin eruptions. He also suffered from recurrent episodes of pneumonia, long-standing atypical predominantly cystic bronchiectasis, and asthma. His total IgE levels were high, peaking at 9,000 IU/ml, and eosinophil counts were also high. *Scedosporium apiospermum*, *Cryptococcus gattii*, and *Aspergillus niger* complex were isolated on multiple occasions. P2 is also colonized with *Stenotrophomonas maltophilia*, and methicillin-resistant *Staphylococcus aureus* has been identified on occasions. P2 has no connective tissue or skeletal abnormalities. Basic immunophenotyping and proliferation assays were normal. STAT1 phosphorylation was normal, and no autoantibodies against gamma-IFN or GM-CSF were detected. Neutrophil function was also normal. Serological tests for HIV were negative. P2 required multiple arterial embolizations for hemoptysis and requires long-term posaconazole prophylaxis for recurrent fungal infections. WES identified a heterozygous nonsense variant, c.1111_1112del, of *STAT3*, which was confirmed by Sanger sequencing. P2 was therefore diagnosed with AD-*STAT3*-HIES.

P3 (kindred C) is a 6-yr-old boy of Indian origin. At the age of 1 yr, he developed watery vesicles all over the body, with fever and itching. Ointments had no effect on the vesicles, which self-resolved, leaving hyperpigmented scars. At the age of 2 yr, P3 suffered pneumonia, with right empyema requiring drainage. The lower lobe of the right lung collapsed. Bronchoalveolar lavage fluid culture yielded *S. aureus*, and test results for TB were negative. P3 developed right lower chest wall and left calf muscle abscesses and also displayed pallor and multiple macular spots on the lower abdomen. HIV tests were negative, and nitroblue tetrazolium reduction test results were normal, as were the results of the dihydrorhodamine assay, a finding not consistent with chronic granulomatous disease. P3 had very high absolute eosinophil counts and high IgE levels (9,752 IU/ml). The other Igs were present at normal levels. P3 presented no atopy, coarse facies, or candidiasis. His NIH score reached 40, and he had low T helper 17 cell levels. HIES was suspected and a genetic study was performed. WES identified a heterozygous nonsense variant, c.1552C>T, of *STAT3*, which was confirmed by Sanger sequencing when the patient was 3 yr old. This variant was not identified in the parents and siblings of P3, suggesting that it was a de novo variant. The patient was diagnosed with AD-*STAT3*-HIES.

P4 (kindred D) is a 51-yr-old man with a typical HIES phenotype, with skin abscesses, pneumonia complicated by cavity aspergillosis, and high IgE levels. He also developed vascular abnormalities, with aneurisms of the aorta and coronary artery. NIH score reached 40. At the age of 41 yr, a heterozygous nonsense variant, c.1685G>A, of *STAT3* was identified by WES and

confirmed by Sanger sequencing. P4 was therefore diagnosed with AD-*STAT3*-HIES. It was recently shown that he had transmitted his *STAT3* nonsense variant to his son (P5). P5 is a 16-yr-old boy diagnosed with AD-*STAT3*-HIES at the age of 14 yr. He suffered recurrent skin abscesses, pneumonia, bacterial infections, and osteopenia. He also had high absolute eosinophil counts and high IgE levels (1,133 IU/ml).

P6 and P7 (kindred E) are of New Zealand Maori descent. In terms of the clinical phenotype of HIES, P6 has suffered inflammatory skin disease since childhood, with pyogenic skin infections, bullous lung disease and bronchiectasis, and recurrent staphylococcal pneumonia and bacteremia. He also has high total IgE level (>50,000 IU/ml). He has no connective tissue features. No clinical information is available for his affected daughter (P7) other than her *STAT3* genotype.

P8 and P9 (kindred F) are of Moroccan origin. We have limited clinical information for these two patients, both of whom have only a mild elevation of IgE levels (P8, 644 IU/ml; P9, 606 IU/ml) and TB infection. P9, who is an affected daughter of P8, died from infection, and we were unable to obtain any other clinical information in support of suspected HIES. WES identified a heterozygous nonsense variant, c.2091delT, of *STAT3* in both patients, which was confirmed by Sanger sequencing. Our studies implicated this variant in HIES on the basis of functional analysis. These two patients were therefore diagnosed with HIES. This variant was not identified in the father and siblings of these patients by Sanger sequencing, suggesting that it was a de novo variant.

P10 (kindred G) is a 13-yr-old boy of Turkish origin. He had no clinical manifestations indicative of a particular susceptibility to bacterial or viral infections. By contrast, he was susceptible to TB infection. His IgE levels were slightly high (961 IU/ml), and his eosinophil count was 4,180/mm^3. We were unable to obtain any information about other clinical manifestations, such as connective tissue signs, that might support a diagnosis of HIES. WES identified a heterozygous nonsense variant, c.2090ins22, of *STAT3*, which was confirmed by Sanger sequencing. This variant has been implicated in HIES on the basis of functional analysis. The patient was therefore diagnosed with AD-*STAT3*-HIES. This variant was not identified in his parents and siblings by Sanger sequencing, suggesting that it was a de novo variant.

Ethics statement

The study was approved by and performed in accordance with the requirements of the institutional ethics committees of The Rockefeller University Hospital, New York, NY; Necker-Enfants Malades Hospital, Paris, France; and the Sydney Local Health District Royal Prince Alfred Hospital Zone Human Research Ethics Committee and Research Governance Office, Royal Prince Alfred Hospital, Camperdown, New South Wales, Australia. Informed consent was obtained for all patients and healthy control volunteers reported in the study.

Genetic analysis

Genomic DNA (gDNA) was prepared from blood samples from patients and controls by the standard phenol-chloroform extraction method. WES was performed with an individual institutional protocol. We performed gDNA extraction, WES data collection, and analysis as previously described (Béziat et al., 2020; Khourieh et al., 2019). Exome capture was performed with the SureSelect Human All Exon 71 Mb kit (Agilent Technologies). Paired-end sequencing was performed on a HiSeq 2500 sequencing system (Illumina) generating 100-base reads. We aligned the sequences with the GRCh37 reference build of the human genome with the Burrows-Wheeler aligner (Li and Durbin, 2010). Downstream processing and variant calling were performed with the Genome Analysis Toolkit (McKenna et al., 2010) and SAMtools (Li et al., 2009). Substitution and insertions/deletions calls were made with the GATK Unified Genotyper. All variants were annotated with annotation software developed in-house (Adzhubei et al., 2010; Kircher et al., 2014; Ng and Henikoff, 2001). For gene-targeting approaches and analysis of familial segregation, exons 2–24 of *STAT3* and their flanking intron sequences were amplified by PCR with specific oligonucleotide primers (available on request). PCR products were purified by centrifugation through Sephadex G-50 Superfine resin (Amersham-Pharmacia-Biotech) and sequenced with the Applied Biosystems Big Dye terminator kit v1.1 (Applied Biosystems) and an ABI Prism 3130xl Analyzer (Applied Biosystems). WES was performed for P1, P2, P3, P4, P6, P8, P9, and P10.

Cell culture, cDNA synthesis, and sequencing

Immortalized SV40 fibroblasts from the patients were grown in complete DMEM supplemented with 10% heat-inactivated FBS. HEK293T cells derived from the human embryonic kidney 293 cell line, which expresses a mutant version of the SV40 large T antigen, were grown in complete DMEM supplemented with 10% FBS. *STAT3*$^{-/-}$ A4 cells derived from human DLD1 colon cancer cells by homologous recombination (Yang et al., 2010) and kindly provided by James E. Darnell, were grown in McCoy's 5A medium containing 10% heat-inactivated FBS. Cells were incubated at 37°C in the presence of 5% CO_2.

mRNA extraction and reverse transcription

Total RNA was extracted from the various cell lines with the RNeasy Plus Mini kit (Qiagen). RNA was then reverse transcribed with SuperScript III reverse transcription (Invitrogen). The cDNA was amplified by PCR with specific oligonucleotide primers (available on request) and sequenced as described above.

Expression vectors and transfection experiments

All *STAT3* variants in our analysis except for D427ins17 (Khourieh et al., 2019) were generated by site-directed mutagenesis. The WT or variant alleles were reintroduced into a Myc-DDK-pCMV6 vector (OriGene). The mutated D427ins17 *STAT3* allele was generated by amplifying the full-length cDNA from patients' EBV-B cells and inserting it into a TOPO cloning plasmid (pCR2.1-TOPO vector; Invitrogen), as described previously (Khourieh et al., 2019). *STAT3*$^{-/-}$ A4 cells and HEK293T cells were transfected with the Myc-DDK-pCMV6 vector, empty or containing the WT or a variant allele, in the presence of

X-tremeGENE 9 DNA Transfection Reagent (Sigma-Aldrich), according to the manufacturer's instructions.

Exon-trapping assay

The exon-trapping assay was performed with a previously described method and vector (Buckler et al., 1991; Burn et al., 1995). *STAT3* gDNA was amplified from control fibroblasts. Each pair of primers (Table S8) was designed to amplify the previous and following exons and introns surrounding the targeted variant exon. Each *STAT3* variant amplified from gDNA was inserted into the pSPL3 plasmid (Life Technologies). Each variant was reintroduced by directed mutagenesis, and the full *STAT3* gDNA fragment was Sanger sequenced. Plasmids were used to transfect Cos-7 cells with the X-tremeGENE 9 DNA Transfection Reagent kit (Sigma-Aldrich) according to the manufacturer's instructions. Cells were harvested 24 h after transfection, and total RNA was extracted as previously described. After cDNA synthesis, PCR was performed with the SD6 (5′-TCTCAGTCA CTGGACAACC-3′) and SA2 (5′-ATCTCAGTGGTATTTGTGAGC-3′) primers for pSPL3 plasmids. The amplified cDNAs were inserted into the pCR4-TOPO plasmid vector (Invitrogen). M13 forward (5′-GTAAAACGACGGCCAG-3′) and M13 reverse (5′-CAGGAA ACAGCTATGAC-3′) primers were used for amplifications for the analysis of potential splicing. We screened 100 colonies for each variant to analyze splicing.

Luciferase reporter assay

The luciferase reporter assay was performed as previously described (Khourieh et al., 2019). Briefly, the reporter vector pGL4.47 (E4041; Promega) contains five copies of the STAT3-responsive element, the sis-inducible element, linked to the luciferase reporter gene *luc2P*. *STAT3*$^{-/-}$ A4 and HEK293T cells were transfected with the pCMV6 vector bearing WT or variant *STAT3* (50 ng), the reporter construct pGL4.47 (200 ng), and an expression vector for *Renilla* luciferase (20 ng), with the X-tremeGENE™ 9 DNA Transfection Reagent kit (Sigma-Aldrich). After 24 h, the transfected cells were left unstimulated or were stimulated with 100 ng/ml recombinant human sIL-6 (8954-SR; R&D Systems) for 24 h. Relative luciferase activity was then determined by normalizing the values against the firefly*Renilla* luciferase signal ratio.

Western blotting

STAT3$^{-/-}$ A4 cells mock transfected or transfected with the empty pCMV6 vector, WT STAT3, or a variant STAT3 were stimulated by incubation with 50 ng/ml sIL-6 for 20 min at 37°C, under an atmosphere containing 5% CO_2. For whole-cell extracts, the cells were lysed by incubation in the following buffer (30 mM Tris, pH 7.5, 2 mM KCl, 2 mM EDTA, and 1% Triton X-100), supplemented with a mixture of protease inhibitors (Sigma-Aldrich) for 30 min at 4°C. The lysates were then centrifuged at 21,000 *g* for 20 min at 4°C. The supernatants were processed directly for Western blotting. Western blotting was performed as previously described (Khourieh et al., 2019; Kong et al., 2010) on 20 µg of total extract from transfected *STAT3*$^{-/-}$ A4 cells, with antibodies against the C terminus (9139; Cell Signaling Technology) or N terminus (sc-8019; Santa Cruz Biotechnology) of the STAT3 protein and Tyr705-phosphorylated STAT3 (9145; Cell Signaling Technology).

Reinitiation analysis

For the R13Vfs* and Q125* alleles, we investigated the site at which translation was reinitiated by mutating the first Met after the premature stop codon in each variant. Directed mutagenesis was performed to change Met residues into Leu or Ala residues for each variant. Each of the reinitiation constructs was used to transfect *STAT3*$^{-/-}$ A4 cells, and Western blotting was performed as described above. Following confirmation of the reinitiation position, selected constructs (Fig. 4 B) were used to transfect *STAT3*$^{-/-}$ A4 cells and HEK293T cells, and luciferase assay were performed.

RNA-seq

EBV-B cells from healthy controls (n = 2), D427ins17 patients (n = 1) who were previously known to have the AD-STAT3-HIES–causing variant with alternative transcript, and AD-STAT3-HIES patients (P3: R518*; n = 1) who we studied herein were analyzed. RNA was extracted with the RNeasy plus micro kit (Qiagen). RNA quality was assessed with the Agilent 2200 TapeStation nucleic acids system. RNA-seq was performed as previously described (Hernandez et al., 2018). In brief, samples were mapped onto the human genome sequence (hg38 assembly) with STAR (Dobin et al., 2013), and counts for the aligned reads for each gene were calculated with HTSeq-count (Anders et al., 2015). RNA-seq datasets for these EBV-B cells have been deposited to the NCBI GEO database under accession numbers GSE153886 (GSM4658112, GSM4658118, and GSM4658124) and GSE149602 (GSM4505723). Sashimi plot analysis was done using Integrative Genomics Viewer (Robinson et al., 2017; Robinson et al., 2011a; Thorvaldsdóttir et al., 2013).

Identification of rare splicing events

Primary fibroblasts from healthy controls (n = 2) and AD-STAT3-HIES patients (P3: R518*, P4: W562*) that are shown to create alternative transcripts in exon trapping were grown in complete DMEM supplemented with 10% FBS for 24 h. Before mRNA extraction, cells were treated by emetine dihydrochloride hydrate (Sigma-Aldrich) 100 µg/ml for 4 h to prevent mRNA decay. mRNA was extracted from primary fibroblasts with TRIzol (Invitrogen) and RNeasy Plus Mini kit (Qiagen) according to the manufacturer's protocol. RNA was then reverse transcribed with SuperScript III reverse transcription (Invitrogen). The full-length cDNA for STAT3 was amplified by PCR with specific oligonucleotide primers (5′-ATGGCCCAATGGAATCAG CTACAG-3′ and 5′-CTCACATGGGGGAGGTAGCG-3′). After fragmentation and library prep, sequence was performed using MiSeq nano sequencing (Illumina) to detect the rare splicing events. These data have been deposited to the Sequence Read Archive (accession no. PRJNA728716).

Prediction software

We used seven software suites to predict the deleteriousness of *STAT3* variants (CADD: https://cadd.gs.washington.edu/score, Condel: http://bbglab.irbbarcelona.org/fannsdb/

signin?next=%2Ffannsdb%2Fquery%2Fcondel, Polyphen2 (PPH2): http://genetics.bwh.harvard.edu/pph2/, Sift: http://sift.jcvi.org/, Mutation Assessor: http://mutationassessor.org/r3/, FATHMM: http://fathmm.biocompute.org.uk/fathmmMKL.htm, and Provean: http://provean.jcvi.org/genome_submit_2.php?species=human).

Online supplemental material

Fig. S1 shows the schematic representation of the exon trapping results for *STAT3* nonsense or frameshift variants. Fig. S2 shows STAT3 transcript analysis by RNA-seq in HIES patients' cells carrying heterozygous *STAT3* nonsense variants. Fig. S3 shows protein expression in *STAT3*$^{-/-}$ A4 cells and STAT3 activity for nonsense or frameshift *STAT3* variants. Fig. S4 shows schematic summary of 150 reported variants, including 8 new *STAT3* variants in HIES. Fig. S5 shows deeper analysis for 20 *STAT3* variants identified as not DN. Table S1 shows a summary of the infectious and clinical phenotypes of patients with *STAT3* nonsense or frameshift variants in our cohort. Table S2 lists canonical and alternative transcripts of *STAT3* nonsense or frameshift variants in HIES. Table S3 lists the summary of 150 reported and new *STAT3* variants. Table S4 shows the correlation between variants consequences and their localization by domain. Table S5 lists the summary of allele activity of both canonical and alternative transcripts for 15 *STAT3* missense variants. Table S6 lists the summary of 14 selected *STAT3* variants from gnomAD database. Table S7 lists the summary of parameters correlated with negative selection. Table S8 lists primer pairs for the exon-trapping assay.

Acknowledgments

We would like to thank the patients and their families for participating in this study. We thank James E. Darnell and Claudia Mertens (The Rockefeller University, New York, NY) for providing the *STAT3*-deficient A4 cell lines. We thank members of the St. Giles Laboratory of Human Genetics of Infectious Diseases Laboratory, Masato Ogishi, Paul Bastard, Peng Zhang, and Yuval Itan for highly pertinent intellectual discussions and suggestions and Yelena Nemirovskaya, Dana Liu, Dominick Papandrea, Mark Woollett, Cécile Patissier, and Tatiana Kochetkov for administrative and technical assistance.

The Laboratory of Human Genetics of Infectious Diseases is supported by the Job Research Foundation, the National Center for Research Resources, and the National Center for Advancing Sciences of the National Institutes of Health Clinical and Translational Science Award program (UL1TR001866); the National Institute of Allergy and Infectious Diseases (P01AI061093); the French National Research Agency (ANR) under the "Investments for the Future" ANR program (ANR-10-IAHU-01), the Integrative Biology of Emerging Infectious Diseases Laboratory of Excellence (ANR-10-LABX-62-IBEID), the "PNEUMOPID" project (ANR 14-CE15-0009-01), and the "ProLegio" project (ANR-15-CE17-0014); the French Foundation for Medical Research (EQU201903007798); the Howard Hughes Medical Institute; The Rockefeller University; the St. Giles Foundation; Institut National de la Santé et de la Recherche Médicale; and the Université de Paris. A.N. Spaan was supported by the European Commission (Horizon 2020 Marie Skłodowska-Curie Individual Fellowship 789645), the Dutch Research Council (Rubicon Grant 019.171LW.015), and the European Molecular Biology Organization (Long-Term Fellowship ALTF 84-2017, nonstipendiary). V. Béziat was supported by the ANR (grant NKIRP-ANR-13-PDOC-0025-01).

Author contributions: T. Asano, J.-L. Casanova, and B. Boisson designed the study and wrote the manuscript. F. Rapaport, V. Béziat, Q. Zhang, A. Puel, and S. Boisson-Dupuis discussed the results and the manuscript. T. Asano, J. Khourieh, P. Zhang, F. Rapaport, S.J. Pelham, J.E. Han, A. Guérin, J. Mackie, D. Hum, T. Habib, and N. Marr performed experiments. T. Asano, J. Khourieh, A. Guérin, J. Mackie, M. Chrabieh, S.G. Tangye, L. Abel, and B. Boisson conducted and analyzed exome analysis. S. Gupta, B. Saikia, J.E.I. Baghdadi, I. Fadil, A. Bousfiha, F. Celmeli, L. Ganeshananadan, J. Peake, L. Droney, A. Williams, N. Hatipoglu, T. Ozcelik, and C. Picard provided material from the patients and conducted clinical explorations. A.N. Spaan, S.J. Pelham, J. Li, and W.-T. Lei provided expertise and feedback. J.-L. Casanova and B. Boisson secured funding. All authors critically reviewed the manuscript.

Disclosures: The authors declare no competing interests exist.

Submitted: 4 December 2020
Revised: 30 March 2021
Accepted: 18 May 2021

References

Abolhassani, H., J. Chou, W. Bainter, C.D. Platt, M. Tavassoli, T. Momen, M. Tavakol, M.H. Eslamian, M. Gharagozlou, M. Movahedi, et al. 2018. Clinical, immunologic, and genetic spectrum of 696 patients with combined immunodeficiency. *J. Allergy Clin. Immunol.* 141:1450–1458. https://doi.org/10.1016/j.jaci.2017.06.049

Adzhubei, I.A., S. Schmidt, L. Peshkin, V.E. Ramensky, A. Gerasimova, P. Bork, A.S. Kondrashov, and S.R. Sunyaev. 2010. A method and server for predicting damaging missense mutations. *Nat. Methods.* 7:248–249. https://doi.org/10.1038/nmeth0410-248

Al Khatib, S., S. Keles, M. Garcia-Lloret, E. Karakoc-Aydiner, I. Reisli, H. Artac, Y. Camcioglu, H. Cokugras, A. Somer, N. Kutukculer, et al. 2009. Defects along the T(H)17 differentiation pathway underlie genetically distinct forms of the hyper IgE syndrome. *J. Allergy Clin. Immunol.* 124: 342–348: 348.e1–348.e5. https://doi.org/10.1016/j.jaci.2009.05.004

Alcántara-Montiel, J.C., T. Staines-Boone, G. López-Herrera, F. Espinosa-Rosales, S.E. Espinosa-Padilla, R. Hernández-Rivas, and L. Santos-Argumedo. 2016. Functional characterization of two new STAT3 mutations associated with hyper-IgE syndrome in a Mexican cohort. *Clin. Genet.* 89:217–221. https://doi.org/10.1111/cge.12658

Anders, S., P.T. Pyl, and W. Huber. 2015. HTSeq--a Python framework to work with high-throughput sequencing data. *Bioinformatics.* 31:166–169. https://doi.org/10.1093/bioinformatics/btu638

Anolik, R., S. Elmariah, S. Lehrhoff, H.J. Votava, F.T. Martiniuk, and W. Levis. 2009. Hyperimmunoglobulin E syndrome with a novel STAT3 mutation. *Dermatol. Online J.* 15:16.

Ashtekar, R., and I. Shah. 2016. Tuberculosis in a case of hyper immunoglobulin E syndrome. *J. Family Med. Prim. Care.* 5:871–872. https://doi.org/10.4103/2249-4863.201167

August, A. 2018. Who regulates whom: ZNF341 is an additional player in the STAT3/T_H17 song. *Sci. Immunol.* 3:eaat9779. https://doi.org/10.1126/sciimmunol.aat9779

Avery, D.T., E.K. Deenick, C.S. Ma, S. Suryani, N. Simpson, G.Y. Chew, T.D. Chan, U. Palendira, J. Bustamante, S. Boisson-Dupuis, et al. 2010. B cell-intrinsic signaling through IL-21 receptor and STAT3 is required for

establishing long-lived antibody responses in humans. *J. Exp. Med.* 207: 155–171. https://doi.org/10.1084/jem.20091706

Béziat, V., J. Li, J.X. Lin, C.S. Ma, P. Li, A. Bousfiha, I. Pellier, S. Zoghi, S. Baris, S. Keles, et al. 2018. A recessive form of hyper-IgE syndrome by disruption of ZNF341-dependent STAT3 transcription and activity. *Sci. Immunol.* 3:eaat4956. https://doi.org/10.1126/sciimmunol.aat4956

Béziat, V., S.J. Tavernier, Y.H. Chen, C.S. Ma, M. Materna, A. Laurence, J. Staal, D. Aschenbrenner, L. Roels, L. Worley, et al. Undiagnosed Diseases Network. 2020. Dominant-negative mutations in human IL6ST underlie hyper-IgE syndrome. *J. Exp. Med.* 217:e20191804. https://doi.org/10.1084/jem.20191804

Boisson, B., Y. Honda, M. Ajiro, J. Bustamante, M. Bendavid, A.R. Gennery, Y. Kawasaki, J. Ichishima, M. Osawa, H. Nihira, et al. 2019. Rescue of recurrent deep intronic mutation underlying cell type-dependent quantitative NEMO deficiency. *J. Clin. Invest.* 129:583–597. https://doi.org/10.1172/JCI124011

Bolze, A., B. Boisson, B. Bosch, A. Antipenko, M. Bouaziz, P. Sackstein, M. Chaker-Margot, V. Barlogis, T. Briggs, E. Colino, et al. 2018. Incomplete penetrance for isolated congenital asplenia in humans with mutations in translated and untranslated *RPSA* exons. *Proc. Natl. Acad. Sci. USA.* 115:E8007–E8016. https://doi.org/10.1073/pnas.1805437115

Borghini, S., S. Tassi, S. Chiesa, F. Caroli, S. Carta, R. Caorsi, M. Fiore, L. Delfino, D. Lasiglié, C. Ferraris, et al. 2011. Clinical presentation and pathogenesis of cold-induced autoinflammatory disease in a family with recurrence of an NLRP12 mutation. *Arthritis Rheum.* 63:830–839. https://doi.org/10.1002/art.30170

Bousfiha, A., L. Jeddane, C. Picard, W. Al-Herz, F. Ailal, T. Chatila, C. Cunningham-Rundles, A. Etzioni, J.L. Franco, S.M. Holland, et al. 2020. Human Inborn Errors of Immunity: 2019 Update of the IUIS Phenotypical Classification. *J. Clin. Immunol.* 40:66–81. https://doi.org/10.1007/s10875-020-00758-x

Buckler, A.J., D.D. Chang, S.L. Graw, J.D. Brook, D.A. Haber, P.A. Sharp, and D.E. Housman. 1991. Exon amplification: a strategy to isolate mammalian genes based on RNA splicing. *Proc. Natl. Acad. Sci. USA.* 88: 4005–4009. https://doi.org/10.1073/pnas.88.9.4005

Buckley, R.H., B.B. Wray, and E.Z. Belmaker. 1972. Extreme hyperimmunoglobulinemia E and undue susceptibility to infection. *Pediatrics.* 49:59–70.

Burn, T.C., T.D. Connors, K.W. Klinger, and G.M. Landes. 1995. Increased exon-trapping efficiency through modifications to the pSPL3 splicing vector. *Gene.* 161:183–187. https://doi.org/10.1016/0378-1119(95)00223-S

Chandesris, M.O., I. Melki, A. Natividad, A. Puel, C. Fieschi, L. Yun, C. Thumerelle, E. Oksenhendler, D. Boutboul, C. Thomas, et al. 2012. Autosomal dominant STAT3 deficiency and hyper-IgE syndrome: molecular, cellular, and clinical features from a French national survey. *Medicine (Baltimore).* 91:e1–e19. https://doi.org/10.1097/MD.0b013e31825f95b9

Choi, Y., and A.P. Chan. 2015. PROVEAN web server: a tool to predict the functional effect of amino acid substitutions and indels. *Bioinformatics.* 31:2745–2747. https://doi.org/10.1093/bioinformatics/btv195

Davis, S.D., J. Schaller, and R.J. Wedgwood. 1966. Job's Syndrome. Recurrent, "cold", staphylococcal abscesses. *Lancet.* 1:1013–1015. https://doi.org/10.1016/S0140-6736(66)90119-X

Dobin, A., C.A. Davis, F. Schlesinger, J. Drenkow, C. Zaleski, S. Jha, P. Batut, M. Chaisson, and T.R. Gingeras. 2013. STAR: ultrafast universal RNA-seq aligner. *Bioinformatics.* 29:15–21. https://doi.org/10.1093/bioinformatics/bts635

Duyk, G.M., S.W. Kim, R.M. Myers, and D.R. Cox. 1990. Exon trapping: a genetic screen to identify candidate transcribed sequences in cloned mammalian genomic DNA. *Proc. Natl. Acad. Sci. USA.* 87:8995–8999. https://doi.org/10.1073/pnas.87.22.8995

Egawa, M., K. Imai, Y. Taketani, T. Morio, and N. Miyasaka. 2019. Two Prenatal Cases of Hyper-IgE Syndrome. *J. Clin. Immunol.* 39:15–18. https://doi.org/10.1007/s10875-018-0588-6

Eilertson, K.E., J.G. Booth, and C.D. Bustamante. 2012. SnIPRE: selection inference using a Poisson random effects model. *PLOS Comput. Biol.* 8: e1002806. https://doi.org/10.1371/journal.pcbi.1002806

Eken, A., M. Cansever, F.Z. Okus, S. Erdem, E. Nain, Z.B. Azizoglu, Y. Haliloglu, M. Karakukcu, A. Ozcan, O. Devecioglu, et al. 2020. ILC3 deficiency and generalized ILC abnormalities in DOCK8-deficient patients. *Allergy.* 75:921–932. https://doi.org/10.1111/all.14081

Engelhardt, K.R., S. McGhee, S. Winkler, A. Sassi, C. Woellner, G. Lopez-Herrera, A. Chen, H.S. Kim, M.G. Lloret, I. Schulze, et al. 2009. Large deletions and point mutations involving the dedicator of cytokinesis 8 (DOCK8) in the autosomal-recessive form of hyper-IgE syndrome. *J. Allergy Clin. Immunol.* 124:1289–302.e4. https://doi.org/10.1016/j.jaci.2009.10.038

Fabre, A., S. Marchal, V. Barlogis, B. Mari, P. Barbry, P.S. Rohrlich, L.R. Forbes, T.P. Vogel, and L. Giovannini-Chami. 2019. Clinical Aspects of STAT3 Gain-of-Function Germline Mutations: A Systematic Review. *J. Allergy Clin. Immunol. Pract.* 7:1958–1969.e9. https://doi.org/10.1016/j.jaip.2019.02.018

Felgentreff, K., M. Siepe, S. Kotthoff, Y. von Kodolitsch, K. Schachtrup, L.D. Notarangelo, J.E. Walter, and S. Ehl. 2014. Severe eczema and Hyper-IgE in Loeys-Dietz-syndrome - contribution to new findings of immune dysregulation in connective tissue disorders. *Clin. Immunol.* 150:43–50. https://doi.org/10.1016/j.clim.2013.11.008

Fleisher, T.A. 2014. Autosomal Recessive Phosphoglucomutase 3 (PGM3) Mutations Link Glycosylation Defects to Atopy, Immune Deficiency, Autoimmunity, and Neurocognitive Impairment. *Pediatrics.* 134(Suppl 3):S181–S182. https://doi.org/10.1542/peds.2014-1817FFFF

Freeman, A.F., E.D. Renner, C. Henderson, A. Langenbeck, K.N. Olivier, A.P. Hsu, B. Hagl, A. Boos, J. Davis, B.E. Marciano, et al. 2013. Lung parenchyma surgery in autosomal dominant hyper-IgE syndrome. *J. Clin. Immunol.* 33:896–902. https://doi.org/10.1007/s10875-013-9890-5

Frey-Jakobs, S., J.M. Hartberger, M. Fliegauf, C. Bossen, M.L. Wehmeyer, J.C. Neubauer, A. Bulashevska, M. Proietti, P. Fröbel, C. Nöltner, et al. 2018. ZNF341 controls STAT3 expression and thereby immunocompetence. *Sci. Immunol.* 3:eaat4941. https://doi.org/10.1126/sciimmunol.aat4941

Fuller, Z.L., J.J. Berg, H. Mostafavi, G. Sella, and M. Przeworski. 2019. Measuring intolerance to mutation in human genetics. *Nat. Genet.* 51: 772–776. https://doi.org/10.1038/s41588-019-0383-1

Ghaffari, J. 2018. Hyperimmunoglobulin E syndrome. *J. Res. Med. Sci.* 23:46. https://doi.org/10.4103/jrms.JRMS_40_18

Giacomelli, M., N. Tamassia, D. Moratto, P. Bertolini, G. Ricci, C. Bertulli, A. Plebani, M. Cassatella, F. Bazzoni, and R. Badolato. 2011. SH2-domain mutations in STAT3 in hyper-IgE syndrome patients result in impairment of IL-10 function. *Eur. J. Immunol.* 41:3075–3084. https://doi.org/10.1002/eji.201141721

González-Pérez, A., and N. López-Bigas. 2011. Improving the assessment of the outcome of nonsynonymous SNVs with a consensus deleteriousness score, Condel. *Am. J. Hum. Genet.* 88:440–449. https://doi.org/10.1016/j.ajhg.2011.03.004

Grimbacher, B., S.M. Holland, J.I. Gallin, F. Greenberg, S.C. Hill, H.L. Malech, J.A. Miller, A.C. O'Connell, and J.M. Puck. 1999. Hyper-IgE syndrome with recurrent infections--an autosomal dominant multisystem disorder. *N. Engl. J. Med.* 340:692–702. https://doi.org/10.1056/NEJM199903043400904

Grimbacher, B., S.M. Holland, and J.M. Puck. 2005. Hyper-IgE syndromes. *Immunol. Rev.* 203:244–250. https://doi.org/10.1111/j.0105-2896.2005.00228.x

Hagl, B., V. Heinz, A. Schlesinger, B.D. Spielberger, J. Sawalle-Belohradsky, M. Senn-Rauh, T. Magg, A.C. Boos, M. Hönig, K. Schwarz, et al. 2016. Key findings to expedite the diagnosis of hyper-IgE syndromes in infants and young children. *Pediatr. Allergy Immunol.* 27:177–184. https://doi.org/10.1111/pai.12512

He, J., J. Shi, X. Xu, W. Zhang, Y. Wang, X. Chen, Y. Du, N. Zhu, J. Zhang, Q. Wang, and J. Yang. 2012. STAT3 mutations correlated with hyper-IgE syndrome lead to blockage of IL-6/STAT3 signalling pathway. *J. Biosci.* 37:243–257. https://doi.org/10.1007/s12038-012-9202-x

Heimall, J., J. Davis, P.A. Shaw, A.P. Hsu, W. Gu, P. Welch, S.M. Holland, and A.F. Freeman. 2011. Paucity of genotype-phenotype correlations in STAT3 mutation positive Hyper IgE Syndrome (HIES). *Clin. Immunol.* 139:75–84. https://doi.org/10.1016/j.clim.2011.01.001

Hernandez, N., I. Melki, H. Jing, T. Habib, S.S.Y. Huang, J. Danielson, T. Kula, S. Drutman, S. Belkaya, V. Rattina, et al. 2018. Life-threatening influenza pneumonitis in a child with inherited IRF9 deficiency. *J. Exp. Med.* 215:2567–2585. https://doi.org/10.1084/jem.20180628

Hillmer, E.J., H. Zhang, H.S. Li, and S.S. Watowich. 2016. STAT3 signaling in immunity. *Cytokine Growth Factor Rev.* 31:1–15. https://doi.org/10.1016/j.cytogfr.2016.05.001

Holland, S.M., F.R. DeLeo, H.Z. Elloumi, A.P. Hsu, G. Uzel, N. Brodsky, A.F. Freeman, A. Demidowich, J. Davis, M.L. Turner, et al. 2007. STAT3 mutations in the hyper-IgE syndrome. *N. Engl. J. Med.* 357:1608–1619. https://doi.org/10.1056/NEJMoa073687

Itan, Y., L. Shang, B. Boisson, E. Patin, A. Bolze, M. Moncada-Vélez, E. Scott, M.J. Ciancanelli, F.G. Lafaille, J.G. Markle, et al. 2015. The human gene damage index as a gene-level approach to prioritizing exome variants. *Proc. Natl. Acad. Sci. USA.* 112:13615–13620. https://doi.org/10.1073/pnas.1518646112

Itan, Y., L. Shang, B. Boisson, M.J. Ciancanelli, J.G. Markle, R. Martinez-Barricarte, E. Scott, I. Shah, P.D. Stenson, J. Gleeson, et al. 2016. The mutation significance cutoff: gene-level thresholds for variant predictions. *Nat. Methods.* 13:109–110. https://doi.org/10.1038/nmeth.3739

Jabara, H.H., D.R. McDonald, E. Janssen, M.J. Massaad, N. Ramesh, A. Borzutzky, I. Rauter, H. Benson, L. Schneider, S. Baxi, et al. 2012. DOCK8 functions as an adaptor that links TLR-MyD88 signaling to B cell activation. *Nat. Immunol.* 13:612–620. https://doi.org/10.1038/ni.2305

Jiao, H., B. Tóth, M. Erdos, I. Fransson, E. Rákóczi, I. Balogh, Z. Magyarics, B. Dérfalvi, G. Csorba, A. Szaflarska, et al. 2008. Novel and recurrent STAT3 mutations in hyper-IgE syndrome patients from different ethnic groups. *Mol. Immunol.* 46:202–206. https://doi.org/10.1016/j.molimm.2008.07.001

Keupp, K., Y. Li, I. Vargel, A. Hoischen, R. Richardson, K. Neveling, Y. Alanay, E. Uz, N. Elcioğlu, M. Rachwalski, et al. 2013. Mutations in the interleukin receptor IL11RA cause autosomal recessive Crouzon-like craniosynostosis. *Mol. Genet. Genomic Med.* 1:223–237. https://doi.org/10.1002/mgg3.28

Khourieh, J., G. Rao, T. Habib, D.T. Avery, A. Lefèvre-Utile, M.O. Chandesris, A. Belkadi, M. Chrabieh, H. Alwaseem, V. Grandin, et al. 2019. A deep intronic splice mutation of *STAT3* underlies hyper IgE syndrome by negative dominance. *Proc. Natl. Acad. Sci. USA.* 116:16463–16472. https://doi.org/10.1073/pnas.1901409116

Kim, H.J., J.H. Kim, Y.K. Shin, S.I. Lee, and K.M. Ahn. 2009. A novel mutation in the linker domain of the signal transducer and activator of transcription 3 gene, p.Lys531Glu, in hyper-IgE syndrome. *J. Allergy Clin. Immunol.* 123:956–958. https://doi.org/10.1016/j.jaci.2009.01.068

Kircher, M., D.M. Witten, P. Jain, B.J. O'Roak, G.M. Cooper, and J. Shendure. 2014. A general framework for estimating the relative pathogenicity of human genetic variants. *Nat. Genet.* 46:310–315. https://doi.org/10.1038/ng.2892

Kong, X.F., M. Ciancanelli, S. Al-Hajjar, L. Alsina, T. Zumwalt, J. Bustamante, J. Feinberg, M. Audry, C. Prando, V. Bryant, et al. 2010. A novel form of human STAT1 deficiency impairing early but not late responses to interferons. *Blood.* 116:5895–5906. https://doi.org/10.1182/blood-2010-04-280586

Kumánovics, A., C.T. Wittwer, R.J. Pryor, N.H. Augustine, M.F. Leppert, J.C. Carey, H.D. Ochs, R.J. Wedgwood, R.J. Faville Jr., P.G. Quie, and H.R. Hill. 2010. Rapid molecular analysis of the STAT3 gene in Job syndrome of hyper-IgE and recurrent infectious diseases. *J. Mol. Diagn.* 12:213–219. https://doi.org/10.2353/jmoldx.2010.090080

Larsen, C.S., M. Christiansen, and T.H. Mogensen. 2019. Autosomal Dominant Hyper-IgE Syndrome Without Significantly Elevated IgE. *J. Clin. Immunol.* 39:827–831. https://doi.org/10.1007/s10875-019-00683-8

Lek, M., K.J. Karczewski, E.V. Minikel, K.E. Samocha, E. Banks, T. Fennell, A.H. O'Donnell-Luria, J.S. Ware, A.J. Hill, B.B. Cummings, et al. Exome Aggregation Consortium. 2016. Analysis of protein-coding genetic variation in 60,706 humans. *Nature.* 536:285–291. https://doi.org/10.1038/nature19057

Li, H., and R. Durbin. 2010. Fast and accurate long-read alignment with Burrows-Wheeler transform. *Bioinformatics.* 26:589–595. https://doi.org/10.1093/bioinformatics/btp698

Li, H., B. Handsaker, A. Wysoker, T. Fennell, J. Ruan, N. Homer, G. Marth, G. Abecasis, and R. Durbin. 1000 Genome Project Data Processing Subgroup. 2009. The Sequence Alignment/Map format and SAMtools. *Bioinformatics.* 25:2078–2079. https://doi.org/10.1093/bioinformatics/btp352

Liu, L., K.M. McBride, and N.C. Reich. 2005. STAT3 nuclear import is independent of tyrosine phosphorylation and mediated by importin-alpha3. *Proc. Natl. Acad. Sci. USA.* 102:8150–8155. https://doi.org/10.1073/pnas.0501643102

Lyons, J.J., Y. Liu, C.A. Ma, X. Yu, M.P. O'Connell, M.G. Lawrence, Y. Zhang, K. Karpe, M. Zhao, A.M. Siegel, et al. 2017. ERBIN deficiency links STAT3 and TGF-β pathway defects with atopy in humans. *J. Exp. Med.* 214:669–680. https://doi.org/10.1084/jem.20161435

Ma, C.S., G.Y. Chew, N. Simpson, A. Priyadarshi, M. Wong, B. Grimbacher, D.A. Fulcher, S.G. Tangye, and M.C. Cook. 2008. Deficiency of Th17 cells in hyper IgE syndrome due to mutations in STAT3. *J. Exp. Med.* 205:1551–1557. https://doi.org/10.1084/jem.20080218

Ma, C.S., D.T. Avery, A. Chan, M. Batten, J. Bustamante, S. Boisson-Dupuis, P.D. Arkwright, A.Y. Kreins, D. Averbuch, D. Engelhard, et al. 2012. Functional STAT3 deficiency compromises the generation of human T follicular helper cells. *Blood.* 119:3997–4008. https://doi.org/10.1182/blood-2011-11-392985

Ma, C.A., J.R. Stinson, Y. Zhang, J.K. Abbott, M.A. Weinreich, P.J. Hauk, P.R. Reynolds, J.J. Lyons, C.G. Nelson, E. Ruffo, et al. 2017. Germline hypomorphic CARD11 mutations in severe atopic disease. *Nat. Genet.* 49:1192–1201. https://doi.org/10.1038/ng.3898

Mather, C.A., S.D. Mooney, S.J. Salipante, S. Scroggins, D. Wu, C.C. Pritchard, and B.H. Shirts. 2016. CADD score has limited clinical validity for the identification of pathogenic variants in noncoding regions in a hereditary cancer panel. *Genet. Med.* 18:1269–1275. https://doi.org/10.1038/gim.2016.44

McKenna, A., M. Hanna, E. Banks, A. Sivachenko, K. Cibulskis, A. Kernytsky, K. Garimella, D. Altshuler, S. Gabriel, M. Daly, and M.A. DePristo. 2010. The Genome Analysis Toolkit: a MapReduce framework for analyzing next-generation DNA sequencing data. *Genome Res.* 20:1297–1303. https://doi.org/10.1101/gr.107524.110

Merli, P., F. Novara, D. Montagna, S. Benzo, M. Tanzi, I. Turin, M. De Amici, A. Merli, O. Zuffardi, and G.L. Marseglia. 2014. Hyper IgE syndrome: anaphylaxis in a patient carrying the N567D STAT3 mutation. *Pediatr. Allergy Immunol.* 25:503–505. https://doi.org/10.1111/pai.12217

Metin, A., G. Uysal, A. Güven, A. Unlu, and M.H. Oztürk. 2004. Tuberculous brain abscess in a patient with hyper IgE syndrome. *Pediatr. Int.* 46:97–100. https://doi.org/10.1111/j.1328-0867.2004.01845.x

Minegishi, Y., M. Saito, S. Tsuchiya, I. Tsuge, H. Takada, T. Hara, N. Kawamura, T. Ariga, S. Pasic, O. Stojkovic, et al. 2007. Dominant-negative mutations in the DNA-binding domain of STAT3 cause hyper-IgE syndrome. *Nature.* 448:1058–1062. https://doi.org/10.1038/nature06096

Minegishi, Y., M. Saito, M. Nagasawa, H. Takada, T. Hara, S. Tsuchiya, K. Agematsu, M. Yamada, N. Kawamura, T. Ariga, et al. 2009. Molecular explanation for the contradiction between systemic Th17 defect and localized bacterial infection in hyper-IgE syndrome. *J. Exp. Med.* 206:1291–1301. https://doi.org/10.1084/jem.20082767

Miyazaki, K., T. Miyazawa, K. Sugimoto, S. Fujita, H. Yanagida, M. Okada, and T. Takemura. 2011. An adolescent with marked hyperimmunoglobulinemia E showing minimal change nephrotic syndrome and a STAT3 gene mutation. *Clin. Nephrol.* 75:369–373. https://doi.org/10.5414/CN106548

Moens, L.N., E. Falk-Sörqvist, A.C. Asplund, E. Bernatowska, C.I. Smith, and M. Nilsson. 2014. Diagnostics of primary immunodeficiency diseases: a sequencing capture approach. *PLoS One.* 9:e114901. https://doi.org/10.1371/journal.pone.0114901

Moens, L., H. Schaballie, B. Bosch, A. Voet, X. Bossuyt, J.L. Casanova, S. Boisson-Dupuis, S.G. Tangye, and I. Meyts. 2017. AD Hyper-IgE Syndrome Due to a Novel Loss-of-Function Mutation in STAT3: a Diagnostic Pursuit Won by Clinical Acuity. *J. Clin. Immunol.* 37:12–17. https://doi.org/10.1007/s10875-016-0351-9

Mogensen, T.H. 2013. STAT3 and the Hyper-IgE syndrome: Clinical presentation, genetic origin, pathogenesis, novel findings and remaining uncertainties. *JAK-STAT.* 2:e23435. https://doi.org/10.4161/jkst.23435

Natarajan, M., A.P. Hsu, M.A. Weinreich, Y. Zhang, J.E. Niemela, J.A. Butman, S. Pittaluga, J. Sugui, A.L. Collar, J.K. Lim, et al. 2018. Aspergillosis, eosinophilic esophagitis, and allergic rhinitis in signal transducer and activator of transcription 3 haploinsufficiency. *J. Allergy Clin. Immunol.* 142:993–997.e3. https://doi.org/10.1016/j.jaci.2018.05.009

Ng, P.C., and S. Henikoff. 2001. Predicting deleterious amino acid substitutions. *Genome Res.* 11:863–874. https://doi.org/10.1101/gr.176601

Noensie, E.N., and H.C. Dietz. 2001. A strategy for disease gene identification through nonsense-mediated mRNA decay inhibition. *Nat. Biotechnol.* 19:434–439. https://doi.org/10.1038/88099

Panopoulos, A.D., L. Zhang, J.W. Snow, D.M. Jones, A.M. Smith, K.C. El Kasmi, F. Liu, M.A. Goldsmith, D.C. Link, P.J. Murray, and S.S. Watowich. 2006. STAT3 governs distinct pathways in emergency granulopoiesis and mature neutrophils. *Blood.* 108:3682–3690. https://doi.org/10.1182/blood-2006-02-003012

Papanastasiou, A.D., S. Mantagos, D.A. Papanastasiou, and I.K. Zarkadis. 2010. A novel mutation in the signal transducer and activator of transcription 3 (STAT3) gene, in hyper-IgE syndrome. *Mol. Immunol.* 47:1629–1634. https://doi.org/10.1016/j.molimm.2010.01.010

Pelham, S.J., H.C. Lenthall, E.K. Deenick, and S.G. Tangye. 2016. Elucidating the effects of disease-causing mutations on STAT3 function in autosomal-dominant hyper-IgE syndrome. *J. Allergy Clin. Immunol.* 138:1210–1213.e5. https://doi.org/10.1016/j.jaci.2016.04.020

Powers, A.E., J.M. Bender, A. Kumánovics, K. Ampofo, N. Augustine, A.T. Pavia, and H.R. Hill. 2009. Coccidioides immitis meningitis in a patient with hyperimmunoglobulin E syndrome due to a novel mutation in signal transducer and activator of transcription. *Pediatr. Infect. Dis. J.* 28:664–666. https://doi.org/10.1097/INF.0b013e31819866ec

Rapaport, F., B. Boisson, A. Gregor, V. Béziat, S. Boisson-Dupuis, J. Bustamante, E. Jouanguy, A. Puel, J. Rosain, Q. Zhang, et al. 2021. Negative selection on human genes underlying inborn errors depends on disease outcome and both the mode and mechanism of inheritance. *Proc. Natl. Acad. Sci. USA.* 118:e2001248118. https://doi.org/10.1073/pnas.2001248118

Renner, E.D., T.R. Torgerson, S. Rylaarsdam, S. Añover-Sombke, K. Golob, T. LaFlam, Q. Zhu, and H.D. Ochs. 2007. STAT3 mutation in the original

patient with Job's syndrome. *N. Engl. J. Med.* 357:1667–1668. https://doi.org/10.1056/NEJMc076367

Renner, E.D., S. Rylaarsdam, S. Anover-Sombke, A.L. Rack, J. Reichenbach, J.C. Carey, Q. Zhu, A.F. Jansson, J. Barboza, L.F. Schimke, et al. 2008. Novel signal transducer and activator of transcription 3 (STAT3) mutations, reduced T(H)17 cell numbers, and variably defective STAT3 phosphorylation in hyper-IgE syndrome. *J. Allergy Clin. Immunol.* 122: 181–187. https://doi.org/10.1016/j.jaci.2008.04.037

Rentzsch, P., D. Witten, G.M. Cooper, J. Shendure, and M. Kircher. 2019. CADD: predicting the deleteriousness of variants throughout the human genome. *Nucleic Acids Res.* 47(D1):D886–D894. https://doi.org/10.1093/nar/gky1016

Reva, B., Y. Antipin, and C. Sander. 2011. Predicting the functional impact of protein mutations: application to cancer genomics. *Nucleic Acids Res.* 39: e118. https://doi.org/10.1093/nar/gkr407

Rieux-Laucat, F., and J.L. Casanova. 2014. Immunology. Autoimmunity by haploinsufficiency. *Science.* 345:1560–1561. https://doi.org/10.1126/science.1260791

Robinson, J.T., H. Thorvaldsdóttir, W. Winckler, M. Guttman, E.S. Lander, G. Getz, and J.P. Mesirov. 2011a. Integrative genomics viewer. *Nat. Biotechnol.* 29:24–26. https://doi.org/10.1038/nbt.1754

Robinson, W.S., S.R. Arnold, C.F. Michael, J.D. Vickery, R.A. Schoumacher, E.K. Pivnick, J.C. Ward, V. Nagabhushanam, and D.B. Lew. 2011b. Case report of a young child with disseminated histoplasmosis and review of hyper immunoglobulin e syndrome (HIES). *Clin. Mol. Allergy.* 9:14. https://doi.org/10.1186/1476-7961-9-14

Robinson, J.T., H. Thorvaldsdóttir, A.M. Wenger, A. Zehir, and J.P. Mesirov. 2017. Variant Review with the Integrative Genomics Viewer. *Cancer Res.* 77:e31–e34. https://doi.org/10.1158/0008-5472.CAN-17-0337

Rogers, M.F., H.A. Shihab, M. Mort, D.N. Cooper, T.R. Gaunt, and C. Campbell. 2018. FATHMM-XF: accurate prediction of pathogenic point mutations via extended features. *Bioinformatics.* 34:511–513. https://doi.org/10.1093/bioinformatics/btx536

Sassi, A., S. Lazaroski, G. Wu, S.M. Haslam, M. Fliegauf, F. Mellouli, T. Patiroglu, E. Unal, M.A. Ozdemir, Z. Jouhadi, et al. 2014. Hypomorphic homozygous mutations in phosphoglucomutase 3 (PGM3) impair immunity and increase serum IgE levels. *J. Allergy Clin. Immunol.* 133: 1410–1419: 1419.e1–1419.e13. https://doi.org/10.1016/j.jaci.2014.02.025

Schimke, L.F., J. Sawalle-Belohradsky, J. Roesler, A. Wollenberg, A. Rack, M. Borte, N. Rieber, R. Cremer, E. Maass, R. Dopfer, et al. 2010. Diagnostic approach to the hyper-IgE syndromes: immunologic and clinical key findings to differentiate hyper-IgE syndromes from atopic dermatitis. *J. Allergy Clin. Immunol.* 126:611–7.e1. https://doi.org/10.1016/j.jaci.2010.06.029

Schwerd, T., S.R.F. Twigg, D. Aschenbrenner, S. Manrique, K.A. Miller, I.B. Taylor, M. Capitani, S.J. McGowan, E. Sweeney, A. Weber, et al. 2017. A biallelic mutation in *IL6ST* encoding the GP130 co-receptor causes immunodeficiency and craniosynostosis. *J. Exp. Med.* 214:2547–2562. https://doi.org/10.1084/jem.20161810

Siegel, A.M., K.D. Stone, G. Cruse, M.G. Lawrence, A. Olivera, M.Y. Jung, J.S. Barber, A.F. Freeman, S.M. Holland, M. O'Brien, et al. 2013. Diminished allergic disease in patients with STAT3 mutations reveals a role for STAT3 signaling in mast cell degranulation. *J. Allergy Clin. Immunol.* 132: 1388–1396.e3. https://doi.org/10.1016/j.jaci.2013.08.045

Spencer, S., S. Köstel Bal, W. Egner, H. Lango Allen, S.I. Raza, C.A. Ma, M. Gürel, Y. Zhang, G. Sun, R.A. Sabroe, et al. 2019. Loss of the interleukin-6 receptor causes immunodeficiency, atopy, and abnormal inflammatory responses. *J. Exp. Med.* 216:1986–1998. https://doi.org/10.1084/jem.20190344

Steward-Tharp, S.M., A. Laurence, Y. Kanno, A. Kotlyar, A.V. Villarino, G. Sciume, S. Kuchen, W. Resch, E.A. Wohlfert, K. Jiang, et al. 2014. A mouse model of HIES reveals pro- and anti-inflammatory functions of STAT3. *Blood.* 123:2978–2987. https://doi.org/10.1182/blood-2013-09-523167

Su, H.C. 2010. Combined immunodeficiency associated with DOCK8 mutations and related immunodeficiencies. *Dis. Markers.* 29:121–122. https://doi.org/10.1155/2010/607891

Sundin, M., B. Tesi, M. Sund Böhme, Y.T. Bryceson, K. Pütsep, S.C. Chiang, S. Thunberg, J. Winiarski, and A.C. Wikström. 2014. Novel STAT3 mutation causing hyper-IgE syndrome: studies of the clinical course and immunopathology. *J. Clin. Immunol.* 34:469–477. https://doi.org/10.1007/s10875-014-0011-x

Tangye, S.G., W. Al-Herz, A. Bousfiha, T. Chatila, C. Cunningham-Rundles, A. Etzioni, J.L. Franco, S.M. Holland, C. Klein, T. Morio, et al. 2020. Human Inborn Errors of Immunity: 2019 Update on the Classification from the International Union of Immunological Societies Expert Committee. *J. Clin. Immunol.* 40:24–64. https://doi.org/10.1007/s10875-019-00737-x

Tavassoli, M., H. Abolhassani, R. Yazdani, M. Ghadami, G. Azizi, S. Abdolrahim Poor Heravi, T. Moeini Shad, M. Kokabee, M. Movahedi, H. Abdshahzadeh, et al. 2019. The first cohort of Iranian patients with hyper immunoglobulin E syndrome: A long-term follow-up and genetic analysis. *Pediatr. Allergy Immunol.* 30:469–478. https://doi.org/10.1111/pai.13043

Thorvaldsdóttir, H., J.T. Robinson, and J.P. Mesirov. 2013. Integrative Genomics Viewer (IGV): high-performance genomics data visualization and exploration. *Brief. Bioinform.* 14:178–192. https://doi.org/10.1093/bib/bbs017

Tsilifis, C., A.F. Freeman, and A.R. Gennery. 2021. STAT3 Hyper IgE syndrome – an update and unanswered questions. *J. Clin. Immunol.* In press. https://doi.org/10.1007/s10875-021-01051-1

van de Veerdonk, F.L., R.J. Marijnissen, L.A. Joosten, B.J. Kullberg, J.P. Drenth, M.G. Netea, and J.W. van der Meer. 2010. Milder clinical hyper-immunoglobulin E syndrome phenotype is associated with partial interleukin-17 deficiency. *Clin. Exp. Immunol.* 159:57–64. https://doi.org/10.1111/j.1365-2249.2009.04043.x

Vaser, R., S. Adusumalli, S.N. Leng, M. Sikic, and P.C. Ng. 2016. SIFT missense predictions for genomes. *Nat. Protoc.* 11:1–9. https://doi.org/10.1038/nprot.2015.123

Vinh, D.C., J.A. Sugui, A.P. Hsu, A.F. Freeman, and S.M. Holland. 2010. Invasive fungal disease in autosomal-dominant hyper-IgE syndrome. *J. Allergy Clin. Immunol.* 125:1389–1390. https://doi.org/10.1016/j.jaci.2010.01.047

Woellner, C., E.M. Gertz, A.A. Schäffer, M. Lagos, M. Perro, E.O. Glocker, M.C. Pietrogrande, F. Cossu, J.L. Franco, N. Matamoros, et al. 2010. Mutations in STAT3 and diagnostic guidelines for hyper-IgE syndrome. *J. Allergy Clin. Immunol.* 125:424–432.e8. https://doi.org/10.1016/j.jaci.2009.10.059

Wolach, O., T. Kuijpers, J. Ben-Ari, R. Gavrieli, N. Feinstein-Goren, M. Alders, B.Z. Garty, and B. Wolach. 2014. Variable clinical expressivity of STAT3 mutation in hyperimmunoglobulin E syndrome: genetic and clinical studies of six patients. *J. Clin. Immunol.* 34:163–170. https://doi.org/10.1007/s10875-014-9988-4

Wu, J., J. Chen, Z.Q. Tian, H. Zhang, R.L. Gong, T.X. Chen, and L. Hong. 2017. Clinical Manifestations and Genetic Analysis of 17 Patients with Autosomal Dominant Hyper-IgE Syndrome in Mainland China: New Reports and a Literature Review. *J. Clin. Immunol.* 37:166–179. https://doi.org/10.1007/s10875-017-0369-7

Yang, J., J. Huang, M. Dasgupta, N. Sears, M. Miyagi, B. Wang, M.R. Chance, X. Chen, Y. Du, Y. Wang, et al. 2010. Reversible methylation of promoter-bound STAT3 by histone-modifying enzymes. *Proc. Natl. Acad. Sci. USA.* 107:21499–21504. https://doi.org/10.1073/pnas.1016147107

Zhang, Q., J.C. Davis, I.T. Lamborn, A.F. Freeman, H. Jing, A.J. Favreau, H.F. Matthews, J. Davis, M.L. Turner, G. Uzel, et al. 2009. Combined immunodeficiency associated with DOCK8 mutations. *N. Engl. J. Med.* 361: 2046–2055. https://doi.org/10.1056/NEJMoa0905506

Zhang, H., H. Nguyen-Jackson, A.D. Panopoulos, H.S. Li, P.J. Murray, and S.S. Watowich. 2010a. STAT3 controls myeloid progenitor growth during emergency granulopoiesis. *Blood.* 116:2462–2471. https://doi.org/10.1182/blood-2009-12-259630

Zhang, Q., J.C. Davis, C.G. Dove, and H.C. Su. 2010b. Genetic, clinical, and laboratory markers for DOCK8 immunodeficiency syndrome. *Dis. Markers.* 29:131–139. https://doi.org/10.1155/2010/972591

Zhang, L.Y., W. Tian, L. Shu, L.P. Jiang, Y.Z. Zhan, W. Liu, X.D. Zhao, Y.X. Cui, X.M. Tang, M. Wang, et al. 2013. Clinical features, STAT3 gene mutations and Th17 cell analysis in nine children with hyper-IgE syndrome in mainland China. *Scand. J. Immunol.* 78:258–265. https://doi.org/10.1111/sji.12063

Zhang, Y., X. Yu, M. Ichikawa, J.J. Lyons, S. Datta, I.T. Lamborn, H. Jing, E.S. Kim, M. Biancalana, L.A. Wolfe, et al. 2014. Autosomal recessive phosphoglucomutase 3 (PGM3) mutations link glycosylation defects to atopy, immune deficiency, autoimmunity, and neurocognitive impairment. *J. Allergy Clin. Immunol.* 133:1400–1409: 1409.e1–1409.e5. https://doi.org/10.1016/j.jaci.2014.02.013

Zhang, P., B. Bigio, F. Rapaport, S.Y. Zhang, J.L. Casanova, L. Abel, B. Boisson, and Y. Itan. 2018a. PopViz: a webserver for visualizing minor allele frequencies and damage prediction scores of human genetic variations. *Bioinformatics.* 34:4307–4309. https://doi.org/10.1093/bioinformatics/bty536

Zhang, Q., B. Boisson, V. Béziat, A. Puel, and J.L. Casanova. 2018b. Human hyper-IgE syndrome: singular or plural? *Mamm. Genome.* 29:603–617. https://doi.org/10.1007/s00335-018-9767-2

JEM

Supplemental material

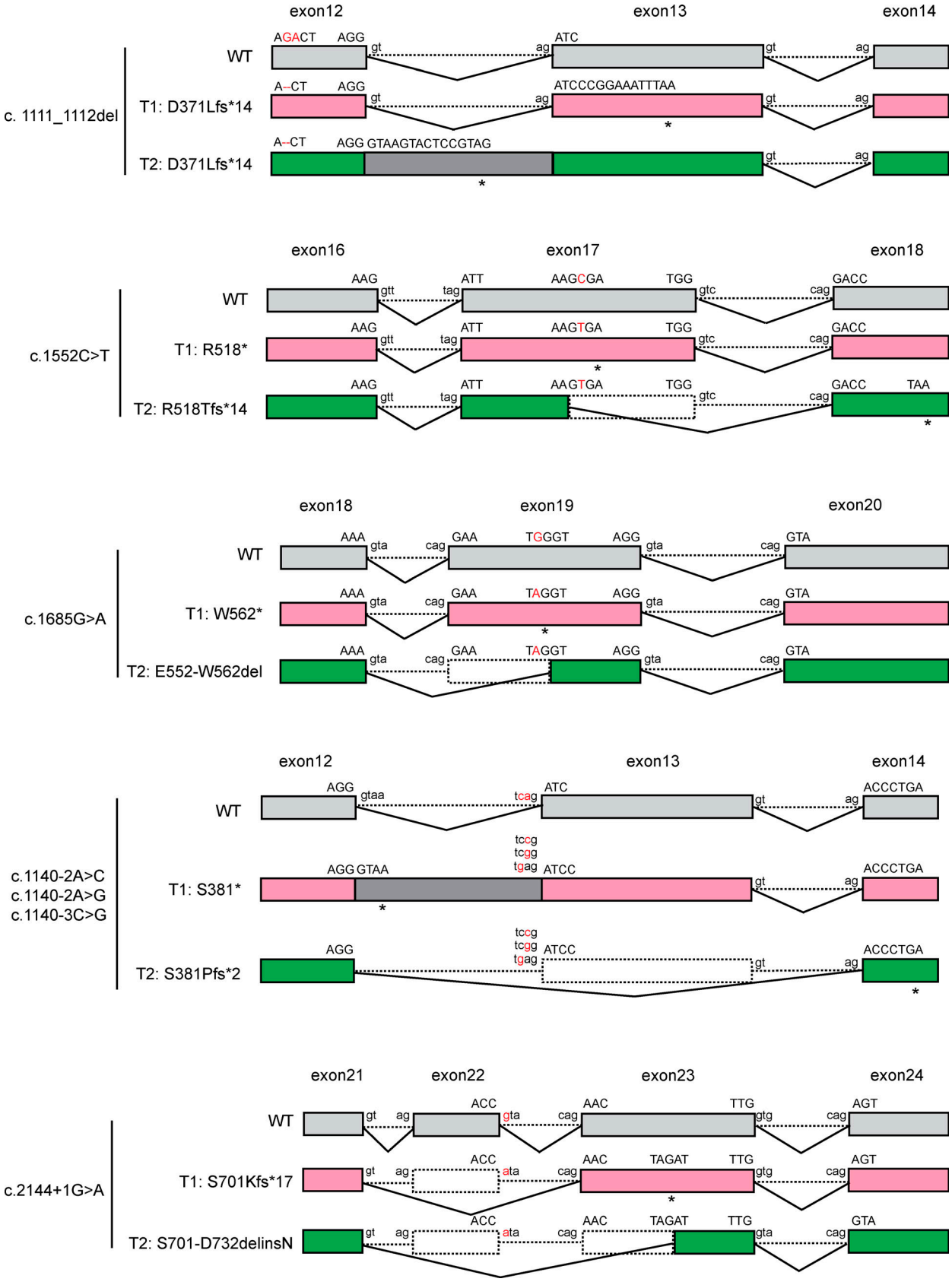

Figure S1. **Schematic representation of the exon-trapping assay for nonsense or frameshift variants.** Schematic representation of variants with alternative transcripts, based on the results of exon-trapping assays. The WT is shown in gray, and the variants are shown in pink and green (T1 in pink and T2 in green). T1 (pink) is the canonical transcript, and T2 (green) is the alternative transcript.

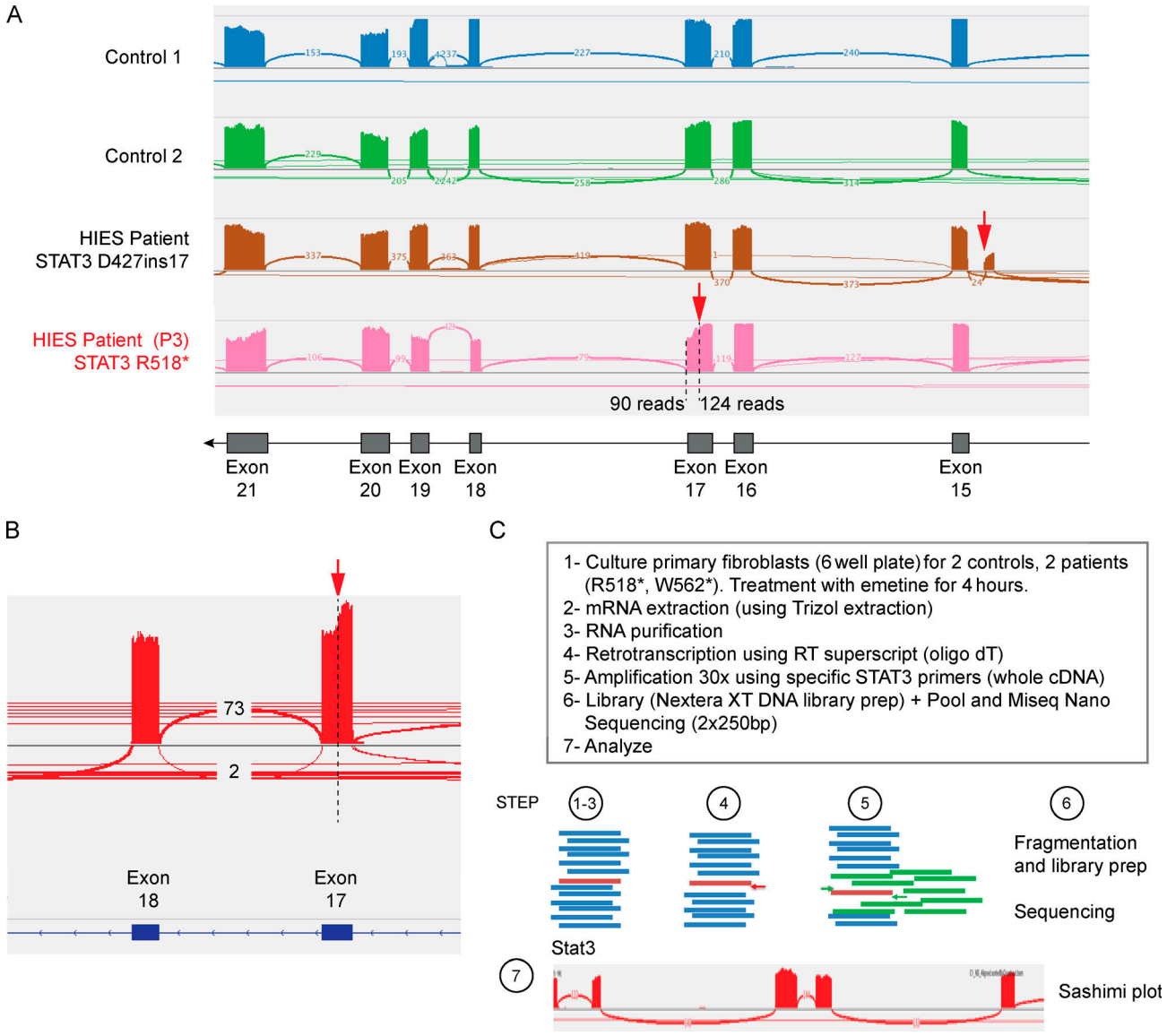

Figure S2. **Deep RNA-seq for the identification of novel alternative splicing in HIES patients' cells with *STAT3* nonsense variants. (A)** RNA-seq results using EBV-B cells derived from HIES patient with *STAT3* nonsense or frameshift variants (P3: R518*). P3 is already shown to have alternative splicing in our exon-trapping system. D427ins17 was previously confirmed to create an alternative transcript (Khourieh et al., 2019) and was used as a positive control. Red arrows represent mutated position. **(B)** RNA-seq result (Sashimi plot) for P3 focusing on the mutated exon. Sashimi plot analysis was demonstrated using Integrative Genomics Viewer. **(C)** Schematic representation of strategy for deep RNA analysis to detect the rare splicing events.

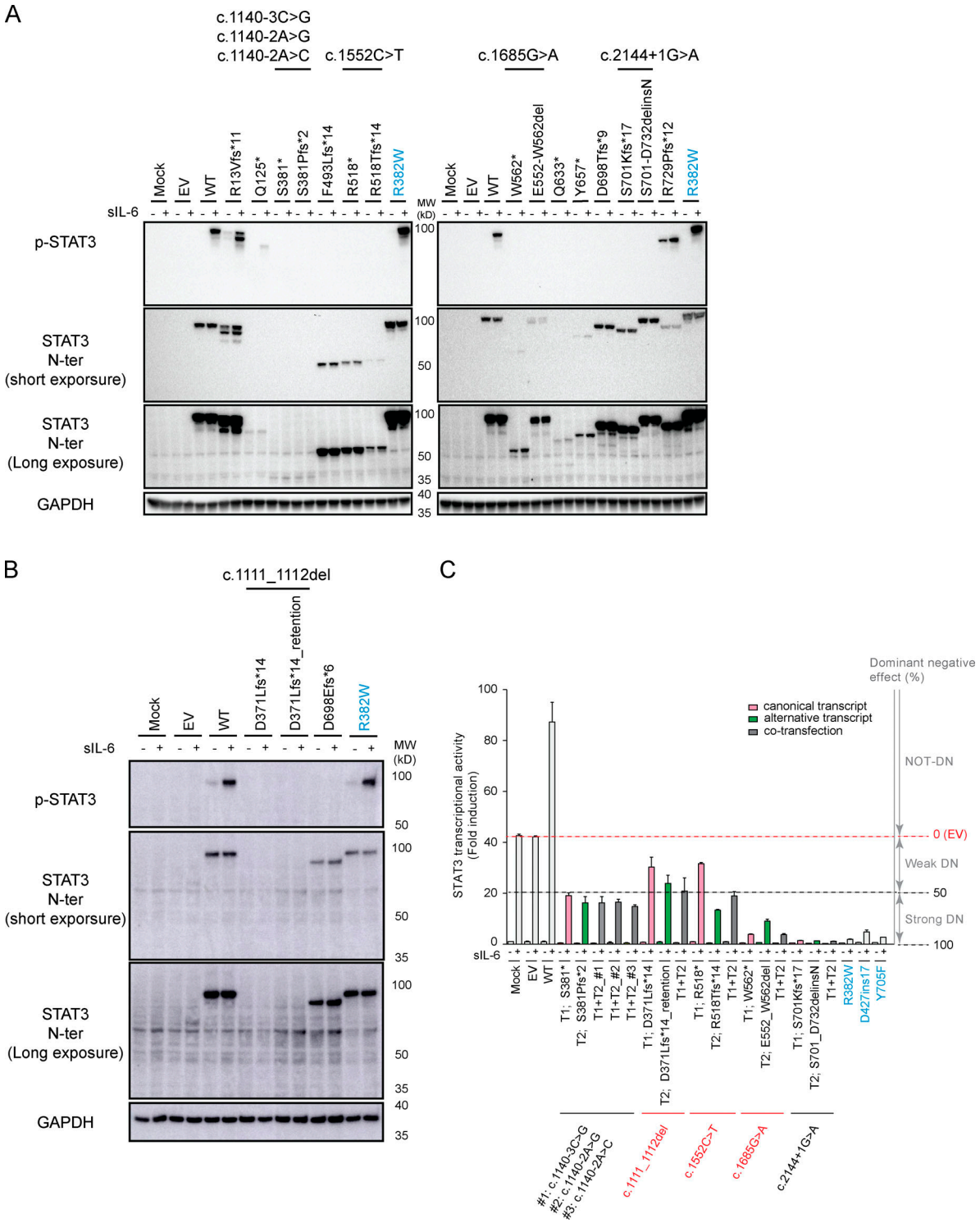

Figure S3. **Protein production and STAT3 activity for nonsense or frameshift *STAT3* variants, taking into account the alternative transcripts. (A and B)** Western blot of extracts from nontransfected *STAT3*$^{-/-}$ A4 cells (mock), A4 cells transfected with pCMV6 EV, the *STAT3* WT allele, or the *STAT3* variant alleles of interest. Total extracts from nontransfected or transfected *STAT3*$^{-/-}$ A4 cells after treatment (+) with 50 ng/ml sIL-6 for 20 min. All extracts probed were with mAbs specific for p-STAT3 or the N-terminal (N-ter) part of the STAT3 protein. **(C)** Luciferase assay on HEK293T cells, which have endogenous STAT3, cotransfected with the canonical transcript and an alternative transcript, according to the ratio estimated in the exon-trapping assay (98% D371LfsX14 [T1] and 2% D371Lfs*14 due to IVS12 retention [T2]; 80% R518* [T1] and 20% R518Tfs* [T2]; 83% W562* [T1] and 17% E552_W562del [T2]; 92% S701Kfs*17 [T1] and 8% S701-D732delinsN [T2]); 52% S381* [T1] and 48% S381Pfs*2 [T2]; and 81% S381* [T1] and 19% S381Pfs*2 [T2]), together with the pGL4.47 reporter construct and an expression vector for *Renilla* luciferase. T1 represents the canonical transcript, and T2 represents alternative transcripts. The red dashed line represents activity after stimulation in EV-transformed cells, and the blacked dashed line represents 50% of this activity. Following cotransfection in the ratios found in exon-trapping assays, all the variants were found to be DN. Each experiment (A–C) was independently performed twice. Error bars represent the means with SEM.

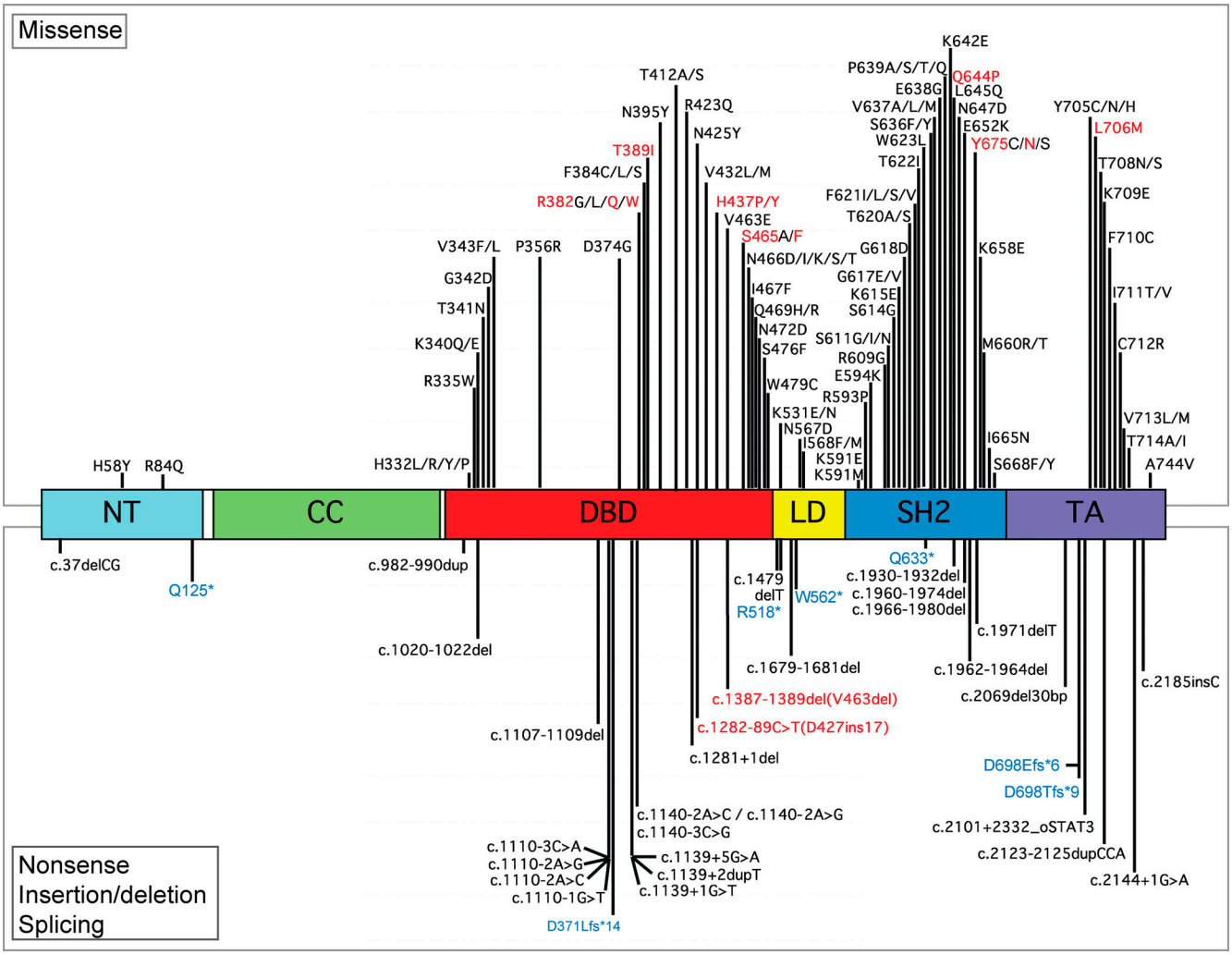

Figure S4. **Summary of 150 reported and new *STAT3* variants in HIES.** Schematic representation of all 150 previously reported and new *STAT3* variants (as of July 1, 2020). Variants in black have been reported before, and those in blue are the new nonsense and frameshift variants identified in our cohorts. The variants in red are the six alleles validated experimentally before this work. Missense variants are described in the upper part of the figure, and nonsense, insertion, deletion, and splicing variants are described in the lower part.

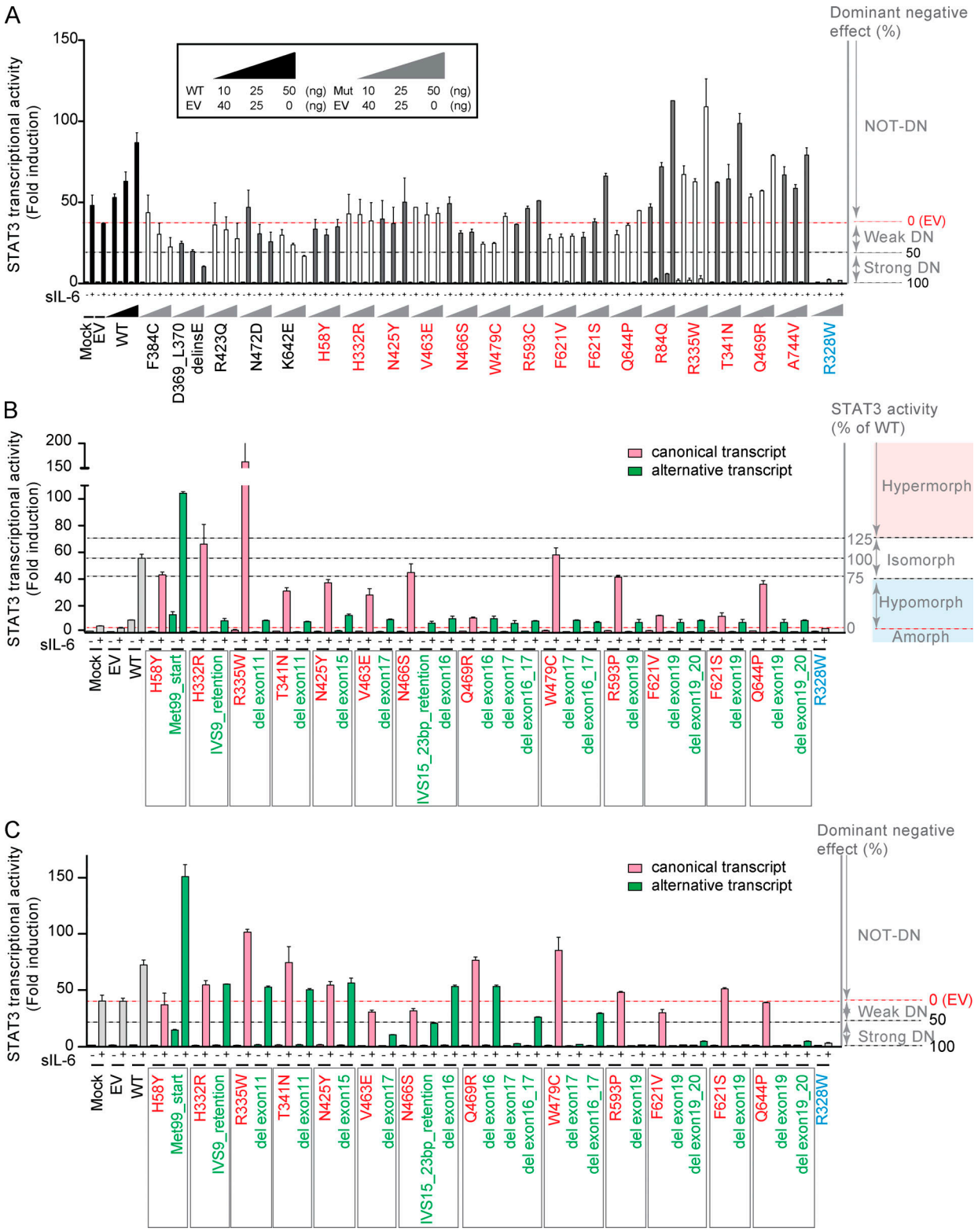

Figure S5. **Analysis for 20 *STAT3* variants identified as not DN in the first luciferase assay. (A)** Dose-dependent mechanism of dominance for 20 *STAT3* variants. Luciferase assay on HEK293T cells, which have endogenous STAT3, transfected with various amounts of WT plasmid or one of the 20 *STAT3* variant plasmids corresponding to variants identified as not DN in Fig. 5 B (both not-DN and weak-DN variants were assigned to this category here). The red dashed line represents stimulated activity in EV-transformed cells, and the black dashed line represents 50% this level of activity. Five variants displayed dose-dependent negative dominance, with a strong or weak DN effect (F384C, D369_L370delinsE, R423Q, N472D, and K642E). The remaining 15 variants (in red) had no DN effect. **(B and C)** 13 of the 15 variants tested generated alternative transcripts (Table S5). Luciferase assay on *STAT3*$^{-/-}$ A4 cells (B) or HEK293T cells (C) transfected with the canonical transcript (pink bar) or alternative transcripts (green bar) were performed to measure STAT3 transcriptional activity. Each experiment (A–C) was independently performed twice. Error bars represent the means with SEM.

Tables S1–S8 are provided online as separate Excel files. Table S1 shows a summary of the infectious and clinical phenotypes of patients with *STAT3* nonsense or frameshift variants in our cohort. Table S2 lists canonical and alternative transcripts of *STAT3* nonsense or frameshift variants in HIES. Table S3 is a summary of the 150 previously reported and new *STAT3* variants and represents all the mutational and functional features studied. Table S4 lists the correlation between variant consequences and their localization by domain for the 150 previously reported and new *STAT3* variants from patients with HIES. Table S5 lists allele activity of canonical and alternative transcripts for 15 *STAT3* missense variants. Table S6 is a summary of 14 selected *STAT3* variants from the gnomAD database. Table S7 lists the summary of parameters correlated with negative selection (*STAT3* and 20 genes displaying HI). Table S8 lists primer pairs for the exon-trapping assay.